Numerical investigation of the seakeeping behavior of a catamaran advancing in regular head waves. Ocean Eng

ARTICLE *in* OCEAN ENGINEERING · NOVEMBER 2011

Impact Factor: 1.35 · DOI: 10.1016/j.oceaneng.2011.09.003

4 AUTHORS:

Teresa Castiglione
Università della Calabria
15 PUBLICATIONS **49** CITATIONS
SEE PROFILE

Frederick Stern
University of Iowa
244 PUBLICATIONS **3,014** CITATIONS
SEE PROFILE

Sergio Bova
Università della Calabria
23 PUBLICATIONS **76** CITATIONS
SEE PROFILE

Manivannan Kandasamy
Flow Inc.
36 PUBLICATIONS **175** CITATIONS
SEE PROFILE

Ocean Engineering 38 (2011) 1806–1822

Contents lists available at SciVerse ScienceDirect

Ocean Engineering

journal homepage: www.elsevier.com/locate/oceaneng

Numerical investigation of the seakeeping behavior of a catamaran advancing in regular head waves

Teresa Castiglione [a,*], Frederick Stern [b], Sergio Bova [a], Manivannan Kandasamy [b]

[a] Department of Mechanical Engineering, Via Pietro Bucci, Cubo 45C, University of Calabria, Arcavacata di Rende, Cosenza, Italy
[b] IIHR-Hydroscience and Engineering, University of Iowa, Iowa City, IA 52242-1585, USA

ARTICLE INFO

Article history:
Received 23 July 2010
Accepted 10 September 2011
Available online 4 October 2011

Keywords:
Seakeeping
RAO
Catamaran
URANS
CFD
Ship motions
Regular waves
Resonance
Wave steepness
Added resistance

ABSTRACT

A numerical study was undertaken in order to assess the capability of an unsteady RANS code to predict the seakeeping characteristics of a high-speed multi-hull vessel in high sea states. Numerical analysis includes evaluation of ship motions, effects of wave steepness on ship response, catamaran natural frequency and added resistance in waves. Computations were performed for the DELFT 372 catamaran by the URANS solver CFDSHIP-Iowa V.4. The code was validated with encouraging results for high ship speeds ($0.3 \le Fn \le 0.75$) and high wave amplitudes ($0.025 \le Ak \le 0.1$). Comparison with strip theory solutions shows that the RANS method predicts ship motions with higher accuracy and allows the detection of nonlinear effects. Current computations evidence that heave peaks occur at resonance for all Fn, and reach the absolute maximum at $Fn=0.75$. Maximum pitch occurs at frequencies lower than resonance, for each speed, and absolute maximum occurs at medium $Fn=0.6$. Maximum added resistance, R_{aw}, was computed at $Fn=0.45$, which, interestingly, is near the catamaran $Fn_{coincidence}$. Overall, we found similar results as Simonsen et al. (2008) for KCS containership, though, herein, a multi-hull geometry and higher speeds were tested. Also, our results are useful to further evaluate the exciting forces and their correlation with f_e and λ/L_{pp}.

1. Introduction

One of the most important aspects of ship design, is to improve the safety and efficiency of ship hulls in response to environmental impact. A ship is, often, optimized in calm water conditions, but a good behavior of the hull in calm water may lead to unwanted behavior in the seaway, where the vessel may be subject to large vertical resonant motions. For this reason, hydrodynamic optimization studies should consider the fundamental aspects of ship analysis as a whole: resistance, propulsion, maneuvering and seakeeping. With particular regard to the seakeeping behavior of a ship, it could be of interest to study the influence of wave amplitudes and lengths on ship motions, on the flow field and on the hydrodynamic forces, in order to predict the range of sea states in which the best performances of the ship can be ensured.

The behavior of ships advancing in waves was traditionally investigated by adopting, mainly, experimental fluid dynamics (EFD) procedures, with focus on the effects of waves on ship motions. O'Dea et al. (1992) presented the results of heave and pitch motions for a containership model, in order to have a better understanding of the linearity of ship response. Nonlinear vertical plane motions were observed for wave steepness values higher than 0.08, while approximately linear response was registered for lower steep waves. Fonseca and Soares (2004) investigated nonlinear vertical plane motions for a model of the ITTC S-175 in regular head waves. Nonlinearities in heave and pitch motions were registered for wave steepness values higher than 0.07 and were more evident near resonance. Recently, Irvine et al. (2008) presented results of coupled heave and pitch motions for a surface combatant, the DTMB 5512, in a range of speeds, wave steepness and wave frequencies, in order to investigate the flow conditions where ship maximum response occurs, and simple equations for estimating the speed of maximum heave and pitch response ($Fn_{coincidence}$) were derived. However, Irvine et al. (2008) were not able to validate the equations, since the test program did not cover speed values higher than $Fn_{coincidence}$. Subsequently, Simonsen et al. (2008) investigated the KCS containership and designed the test program specifically to cover the maximum response conditions predicted by equations. EFD results from Simonsen et al. (2008) partially agree with Irvine et al. (2008).

The early applications of computational fluid dynamics (CFD) to seakeeping problems, involved solution techniques based on the assumptions of potential flows coupled with small amplitude motions. The strip theory for heave and pitch motions in head waves is due to Korvin-Kroukovsky and Jacobs (1957). It was the first motion theory suitable for numerical computations, which

* Corresponding author. Tel.: +39 0984 494162.
E-mail address: teresa.castiglione@unical.it (T. Castiglione).

0029-8018/$ - see front matter © 2011 Elsevier Ltd. All rights reserved.
doi:10.1016/j.oceaneng.2011.09.003

Nomenclature

a	dimensional wave amplitude
A	area, non-dimensional wave amplitude
Ak	wave steepness
A_3	heave motion amplitude
A_{33}	heave added mass
A_5	pitch motion amplitude
A_{55}	pitch added inertia
A_W	waterplane area
B	model beam
C_B	block coefficient
C_D	drag coefficient
CF	correction factor
CFD	computational fluid dynamics
CG	center of gravity
C_T	total resistance coefficient
C_{33}	restoring heave force ($=\rho g A_W$)
C_{55}	restoring pitch moment ($=\rho g I_T$)
D	ship displacement, benchmark data
E	comparison error
EFD	experimental fluid dynamics
f	non-dimensional encounter frequency ($f=(1/\Lambda)+(1/Fn\sqrt{2\pi\Lambda})$)
f_e	ship encounter frequency ($f_e=\sqrt{(g/2\pi\lambda)}+(U/\lambda)$)
f_n	ship natural frequency
Fn	Froude Number
$Fn_{coincidence}$	coincidence Froude number ($f_e=f_n$ and $\lambda/L_{pp}=1.33$)
FS	factor of safety
g	gravity constant (9.81 m/s^2)
I_T	moment of inertia of water plane
I_{55}	mass moment of inertia respect to y axis
k	wave number ($=2\pi/\lambda$)
L_{PP}	model length
m	mass of the vessel
p	pressure distribution
p_{th}	estimated order of accuracy
p_{RE}	order of accuracy computed by Richardson extrapolation
R	ratio between solution changes
R_{aw}	added resistance
R_{T0}	resistance in waves (mean value)
$R_{Tcalmwater}$	steady resistance
r	refinement ratio
$RANS$	Reynolds averaged Navier–Stokes
S_i	numerical solution
T	model draft, wave period
t	time
(U,V,W)	Reynolds-averaged velocity components
U_0	reference ship speed
U_D	experimental data uncertainty
U_{FS}	FS method uncertainty
U_G	grid uncertainty
U_I	iterative uncertainty
U_T	time-step uncertainty
U_{SN}	simulation numerical uncertainty
U_V	validation uncertainty
(x,y,z)	non-inertial ship-fixed coordinates
$x_i(t)$	generic ship degree of freedom
x_{31}	first harmonic amplitude of heave motion
x_{51}	first harmonic amplitude of pitch motion
$\delta_{(t,\ G,\ I,\ RE)}$	numerical error (time, grid, iterative computed by Richardson extrapolation)
ε_{ij}	change between solutions i and j
ϕ_{3_1}	first harmonic heave phase
ϕ_{5_1}	first harmonic pitch phase
λ	dimensional wavelength
Λ	non-dimensional wavelength
τ	time variable non-dimensionalized with wave period
$\zeta(x,t)$	wave elevation
ω_3	heave pulsation ($=2\pi f_{e,3}$)
ω_5	pitch pulsation ($=2\pi f_{e,5}$)

could predict ship motions with high accuracy, though the forward speed terms in the coefficients of the equations of motions did not satisfy the symmetry conditions proved by Timman and Newman (1962). Several attempts were made to improve the Korvin-Kroukovsky and Jacobs theory and new strip theories were also developed (Ogilvie and Tuck, 1969; Salvesen et al., 1970). Salvesen et al. (1970) introduced a new strip theory that could predict heave, pitch, sway, roll and yaw, assuming potential flows, linear and harmonic oscillatory motions and ship lateral symmetry. By this approach, the fully nonlinear governing equations of ship motions were simplified in two sets of coupled linear differential equations: one set of equations for heave and pitch motions and the other set for horizontal plane motions, i.e. sway, yaw and roll. Computations presented by using this approach for several hull shapes, were compared against experimental data and satisfactory agreement was observed both for heave and pitch motions and for vertical and horizontal wave-induced loads. On the contrary, due to the lack of experimental data for horizontal plane motions, the accuracy in predicting sway, yaw and roll was not demonstrated. However, in general, poor accuracy was reached in further strip theory based computations for horizontal plane motions, particularly for roll motion, due to its viscous nature. In order to overcome the limitations of strip theory, attempts to develop numerical methods for viscous flows and large amplitude motions have been made. Currently, research effort is devoted to the application of Reynolds averaged Navier–Stokes (RANS) methods in seakeeping and maneuvering problems, since effects due to viscosity and turbulence are implicitly included in the flow equations. Numerical simulations based on Navier–Stokes solvers, have achieved high accuracy in problems involving steady resistance and propulsion in calm water (Larsson et al., 2000). On the contrary, much effort is required to apply and extend the use of RANS methods in seakeeping and maneuvering, due to the complexity of simulating unsteady flows and ship motions. Several attempts to develop CFD methods for predicting ship motions in the vertical plane, for a ship advancing in waves, can be found in the literature with encouraging results. Some of them include Sato et al. (1999), who computed heave and pitch motions for the Wigley hull and the Series 60, introducing a density function method to model the free surface and a ship-fixed coordinate system to compute ship motions in regular head waves. Cura Hochbaum and Vogt (2002) performed computations for the Series60 and for a C-Box container ship free to surge, heave and pitch in waves and used a two-phase level-set method to compute the free surface flow. Good agreement between the computations and the experimental data at small wave amplitudes, was achieved. Also Orihara and Miyata (2003) obtained promising results in the computations of heave and pitch motions for a container ship and emphasized on added mass and on motions transfer functions. They introduced a density function method to model the free surface and an overlapping grid system to implement the interaction of ships with incident waves and the resultant ship motions. In the mentioned works, however,

the validation against experimental data was limited. Wilson et al. (2005) performed simulations for predicted and prescribed roll motion for the surface combatant DTMB 5512 by a RANS code, which included a surface tracking technique to compute the free surface. A verification and validation study was performed, in order to quantify numerical and modeling errors and the comparison with experiments showed very good agreement. A detailed analysis of vertical plane motions, by the use of a surface tracking RANS code, is found in Weymouth et al. (2005), where the forward-speed diffraction problem, forward radiation and predicted motion response for the modified Wigley hull in regular head seas, were modeled, and comparison with results from strip theory was also presented. Comparison with experiments, for a wide range of frequencies and Froude numbers, showed good agreement. However, in the mentioned works, ship motions were limited to small amplitudes, mainly owing to the limitations present in the technique used to model the free surface. In fact, a surface-tracking method was used, which fails when excessive grid deformation occurs. Carrica et al. (2006) presented unsteady RANS simulations of the ship forward speed diffraction problem for the DTMB 5512, for which detailed experimental data are available, and a surface capturing single-phase level set method was developed for the computation of the free surface. Subsequently, the same method was extended to include six degrees of freedom (6DOF) motions using overset grids moving with relative motions during the computation (Carrica et al., 2007b). Pitch and heave motions were computed for the DTMB model 5521, at $Fn=0.28$ and 0.41 in regular head waves with $\lambda/L=1.5$ and $Ak=0.025$. The predicted motions compared favorably with existing experimental data and a verification and validation analysis was also performed. A solution for a large amplitude head wave case ($Ak=0.075$) was also obtained, in which large amplitude nonlinear motions and transom wave-breaking phenomena were observed. Recently, Mousaviraad et al. (2010) developed a harmonic wave group (HWG) single run seakeeping procedure, by using an unsteady RANS solver. Heave and pitch motions amplitudes and phases were computed for the DTMB 5512 advancing in head waves and the results, achieved by the use of the HWG procedure, were compared with the regular wave (RW) procedure, which requires multiple runs, and with the transient wave group (TWG) technique. Heave and pitch motions were quite well predicted, with average errors of 3.08%D, 3.39%D and 4.35%D for regular waves, harmonic wave group and transient wave group, respectively. The computations proved the greater accuracy of the regular waves results, but with small differences with respect to the harmonic wave group results. Furthermore, the HWG technique was shown to be the most efficient in that it saved 75.8% on the computational cost compared to the RW procedure and 39% compared to the TWG technique.

This paper discusses CFD results for a high-speed multi-hull ship advancing in regular waves, and includes a rigorous verification and validation (V&V) study, comparison with experimental data and strip theory, evaluation of natural frequencies and maximum response, effects of wave steepness, Ak, and evaluation of added resistance. Simulations were performed with an Unsteady Reynolds-Average Navier–Stokes (URANS) code for a high-speed catamaran. The maximum response conditions for the catamaran were investigated, with consideration to resonance and λ/L_{PP} conditions. The effects of wave steepness on nonlinearities of heave and pitch motions were investigated for selected conditions ($Ak=0.025$, 0.05 and 0.1), although experimental data are available for $Ak=0.025$. Heave and pitch motions were compared to linear strip theory results performed by VERES software (2003). Finally, results on added resistance in waves are presented with focus on maximum R_{aw} and its correlation with the coincidence Froude number, $Fn_{coincidence}$.

2. Computational method

The code CFDSHIP-Iowa V.4, used herein, is an unsteady RANS code developed for ship hydrodynamics, and is intended for steady and unsteady computations. A more detailed description of the solver can be found in Carrica et al. (2007a,b) and in Xing et al. (2008).

Briefly, the unsteady Reynolds Averaged Navier–Stokes equations are solved for the liquid phase of a free surface flow, in an absolute inertial earth-fixed reference frame (X,Y,Z), for an arbitrary moving but non-deforming control volume and solution domain (Fig. 1). The free surface is captured using a single-phase level-set method (Carrica et al., 2007a) and a blended k–ε/k–ω model without wall functions models turbulence. The equations are discretized in space using a finite difference approach. Convective terms use second-order upwind schemes and the diffusion terms use second-order central differences. Temporal terms are discretized using a second-order backwards Euler scheme. A PISO algorithm is used to enforce mass conservation, resulting in the Poisson equation for pressure. CFDSHIP-Iowa allows overset multiblock grids and in particular the SUGGAR code (Noack, 2005) is used to obtain the overset domain connectivity between the set of overlapping grids.

At each time step, the fluid flow equations are solved, and, by integrating the elemental forces, the forces and moments acting on the ship are computed and projected in a non-inertial ship-fixed reference frame (x,y,z), with its origin, o, fixed at the center of gravity of the ship. By the application of the rigid body equations, the translational and angular velocities of the ship are computed using a predictor/corrector approach. Rigid overset grids move with relative motion during computations and the interpolation coefficients between the grids are recomputed dynamically, every time the grids move. Around 2–5 nonlinear iterations are performed for convergence of the flow field equations and of ship motions equations within each time step.

In the following equations, which model the initial and inlet boundary conditions for problems involving sinusoidal incident waves, all variables are non-dimensionalized with ship length, L_{pp}, and ship speed, U. Time, t, is non-dimensionalized with wave period, T. At inlet, the time varying incident wave elevation, $\zeta_I(x,\tau)$, in the longitudinal direction, x, with amplitude A ($A=a/L_{PP}$)

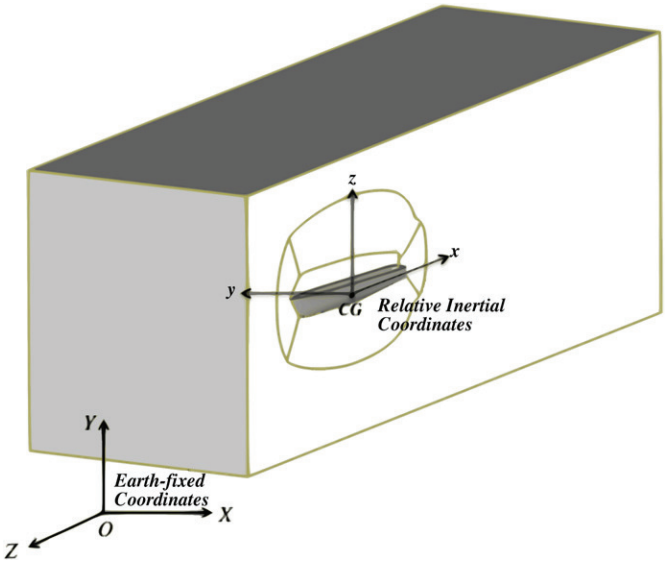

Fig. 1. Definition of the absolute inertial earth-fixed coordinates (X,Y,Z) and non-inertial ship-fixed coordinates (x,y,z) with origin o in the ship center of gravity.

and wavelength Λ ($\Lambda=\lambda/L_{pp}$), is imposed and is given by:

$$\zeta_I(x,\tau)=A\cos[kx-2\pi f\tau] \quad (1)$$

The wave velocity components in the (x,y,z) directions are U, V and W, respectively:

$$U(x,y,z,\tau)=U_0+\frac{A}{Fn}\sqrt{k}e^{kz}\ \cos\left[kx-2\pi f\tau\right] \quad (2)$$

$$V(x,y,z,\tau)=0 \quad (3)$$

$$W(x,y,z,\tau)=\frac{A}{Fn}\sqrt{k}e^{kz}\ \sin\left[kx-2\pi f\tau\right] \quad (4)$$

Finally, the water pressure, p, is defined as:

$$p(x,y,z,\tau)=\frac{A}{Fn^2}e^{kz}\left\{\cos\left[kx-2\pi f\tau\right]-\frac{1}{2}\frac{A}{k}e^{kz}\right\} \quad (5)$$

Here, $Fn=U/\sqrt{gL}$ is the Froude number, $k=(2\pi/\Lambda)$ is the wave number and $f=(1/\Lambda)+(1/(Fn\sqrt{2\pi\Lambda}))$ is the non-dimensional encounter frequency.

3. Numerical modeling

3.1. Geometry and test conditions

The tested geometry is the DELFT catamaran model 372 (Fig. 2), designed at DELFT University of Technology (Van't Veer (1998a, b)), for which experimental data are available both in calm water and in regular waves. The lines plan is plotted in Fig. 3 and the main geometric characteristics are summarized in Table 1.

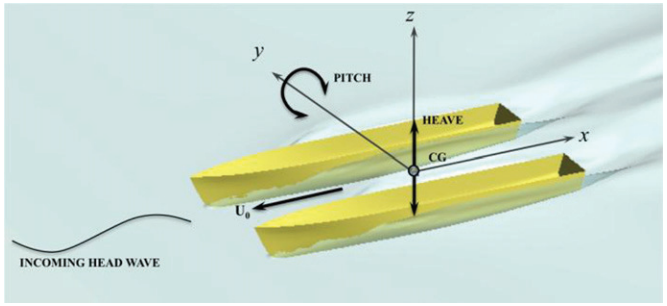

Fig. 2. The catamaran advances in regular head waves at constant forward speed, U_0. The ship responds with unsteady heave and pitch motions. CG indicates the catamaran center of gravity, which is the origin of a ship-fixed reference frame.

Experiments with the 372 catamaran model were carried out in the Delft Ship Hydrodynamic Laboratory of the Delft University of Technology, in a towing tank with dimensions $L\times B\times D=145\times 4.2\times 2.6$ m. Experimental data include resistance, sinkage and trim for the catamaran advancing in calm water, at constant speeds ranging from $Fn=0.18$–0.75. The experiments in regular head waves include heave and pitch amplitudes and phases for speeds ranging from $Fn=0.30$–0.75. The wavelengths are within $\lambda/L_{pp}=0.6$–2. Data include low wave steepness values ($0.015\leq Ak<0.03$).

The unsteady simulations, presented in this work, cover, to a large extent, the EFD test matrix. The flow conditions, in fact, include $Fn=0.3$, 0.45, 0.6, 0.75 and wavelengths ranging from $\lambda/L_{pp}=0.9$–2. In this operating range, the effects of resonance and exciting forces due to the incoming wave, on maximum response of the catamaran, are expected. The test matrix includes steady cases too, for a speed range varying from $Fn=0.3$–0.75, in order to investigate the added resistance in waves. The numerical test conditions are summarized in Table 2.

A numerical study was also undertaken in order to evaluate the linearity of heave and pitch responses with wave amplitude. A high-speed case ($Fn=0.75$) was studied with steeper incoming waves. Specifically, the wave steepness values corresponding to $Ak=0.05$–0.1 were chosen, though experimental data lack for validation. The test conditions are summarized in Table 3.

3.2. Grids and time steps

The computational domain includes a background orthogonal grid, where the far-field boundary conditions are imposed, and a boundary-layer curvilinear grid conforming to ship geometry,

Table 1
Main design parameters of the DELFT catamaran geometry.

Main particulars	Units	Value
Length overall, L_{OA}	m	3.11
Length between perpendiculars, L_{PP}	m	3
Beam overall, B	m	0.94
Beam demihull, b	m	0.24
Distance between center of hulls, H	m	0.7
Draught, T	m	0.15
Displacement, D	kg	87.07
Draught AP, T_{AP}	m	0.15
Draught FP, T_{FP}	m	0.15
Vertical center of gravity, KG	m	0.34
Longitudinal center of gravity, LCG	m	1.41

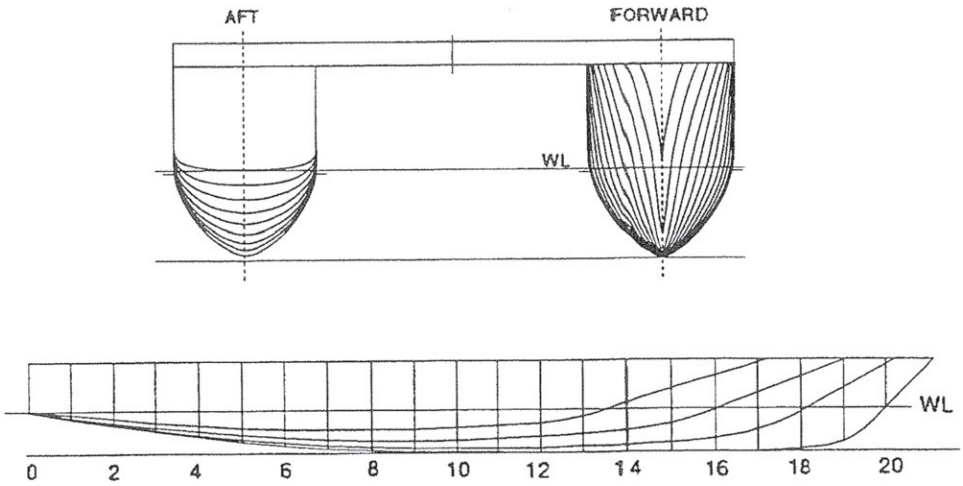

Fig. 3. Lines Plan of DELFT catamaran; WL indicates the waterline.

Table 2
Test matrix for heave and pitch motions.

Fn	Steepness	λ/L_{pp}	Enc. frequency (Hz)
0.3	0.0427	0.899	1.364
0.3	0.0447	0.965	1.296
0.3	0.0323	1.204	1.108
0.3	0.0288	1.301	1.049
0.3	0.0219	1.803	0.838
0.3		Calm water	
0.45	0.030	1.001	1.53
0.45	0.030	1.201	1.33
0.45	0.027	1.396	1.19
0.45	0.025	1.595	1.08
0.45	0.020	1.991	0.92
0.45		Calm water	
0.6	0.030	1.393	1.44
0.6	0.026	1.49	1.319
0.6	0.025	1.6	1.25
0.6	0.021	1.795	1.14
0.6	0.021	1.977	0.9
0.6		Calm water	
0.75	0.025	1.596	1.42
0.75	0.022	1.806	1.287
0.75	0.015	1.983	1.196
0.75	0.015	2.102	1.183
0.75		Calm water	

Table 3
Test matrix for the evaluation of steepness effects on ship motions.

Fn	Steepness	λ/L_{pp}
0.75	0.025	1.596–1.806–1.983–2.012
0.75	0.05	1.596–1.806–1.983–2.012
0.75	0.1	1.596–1.806–1.983–2.012

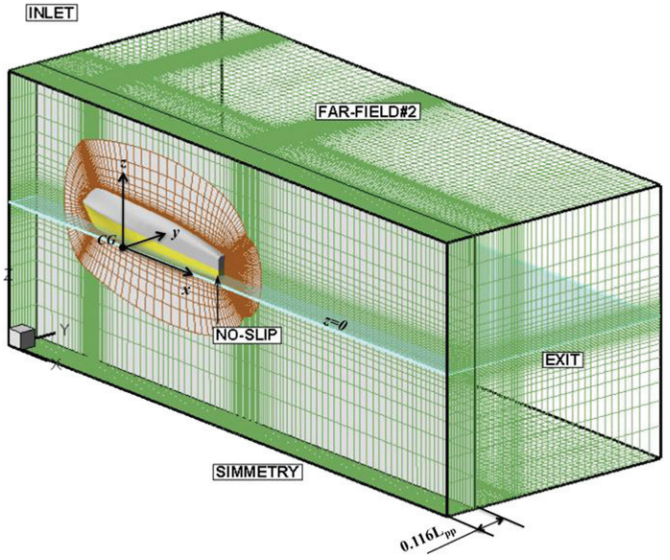

Fig. 4. Computational domain. $y=0$ is the symmetry plane, hence the computational domain includes only one hull. The hull is located at a distance of 0.116 L_{pp} (semi-distance between both hulls) with respect to the symmetry plane.

fully immersed in the background (Fig. 4). The background grid extends in the range $-1 \le x \le 2.5$, $0 \le y \le 1.3$, $-0.65 \le z \le 0.65$, where x, y and z are the ship-fixed non-dimensional coordinates, normalized by ship length, L_{pp}. The ship axis is aligned with the x-axis, with the bow at $x=-0.47$ and the stern at $x=0.53$. The free surface, at rest, lies at $z=0$. The problem solution allows the use of

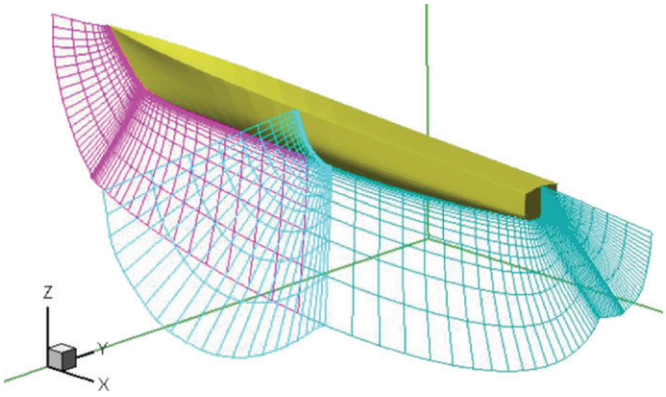

Fig. 5. Body-fitted grid.

a symmetry boundary condition at the centerplane, $y=0$, and half domain has been computed. In the longitudinal direction, the grid is refined at the bow and stern and includes at least 60 grid points per wavelength. This condition is satisfied for the range of wavelengths under consideration. Since the highest waves amplitude of the incident wave is $A=0.04$, in the vertical direction the grid is clustered within $-0.05 \le z \le 0.05$, allowing the computation of larger and smaller amplitude waves. The Cartesian background grid size is 3.8 M points in 8 blocks. The boundary-layer grid (Fig. 5) has a double-O topology. The grid spacing at the hull is set to $y=10^{-5}$ to yield $y^+ < 1$ for the highest Reynolds number case. The grid comprises 1.6 M points in 8 blocks.

The time step size, Δt, was chosen in order to have at least 80 time steps per wave period, which varies with ship speed and wavelength. Therefore, values ranging from $\Delta t=0.00497$–0.01 were fixed in the computations.

4. Verification and validation

To quantify errors and uncertainties in CFD simulations, verification and validation (V&V) was performed following the approach presented in Stern et al. (2006), including the factor of safety (FS) methodology (Xing and Stern, 2010) for convergence study.

Numerical errors and uncertainties are due to the numerical solution of the mathematical equations and include discretization errors, computer round-off errors, artificial dissipation and incomplete iterative and grid convergence. Verification procedure provides an estimation of the numerical errors, given by the sum of the iterative errors and of grid and time-step spacing errors. A minimum of three solutions is required to evaluate convergence with respect to the input parameters, so that the solutions changes for medium-fine, $\varepsilon_{21}=S_2-S_1$, and coarse-medium, $\varepsilon_{32}=S_3-S_2$, solutions are computed. By the evaluation of their ratio, $R=\varepsilon_{21}/\varepsilon_{32}$, the following convergence conditions are possible: (i) monotonic convergence ($0<R<1$); (ii) oscillatory convergence ($R<0$) and (iii) divergence ($R>1$). For monotonic convergence (i), the order of accuracy, p_{RE}, and the error, δ_{RE}, are computed using the Richardson extrapolation (RE) method. For numerical uncertainties, several methods can be used, including the correction factor (CF) method and the factor of safety (FS) method. Within the last method, a better distance metric, P, to the asymptotic range is used instead of the correction factor and is defined as the ratio of p_{RE} to p_{th}:

$$P = \frac{p_{RE}}{p_{th}} \tag{6}$$

When the solutions are in the asymptotic range, then $p_{RE}=p_{th}$; however, in many circumstances, solutions are far from the

asymptotic range such that p_{RE} is greater or smaller than p_{th}. One of the improvements of the FS method, with respect to the CF method, is that it overcomes the too small uncertainty estimates for $p_{RE} > p_{th}$. Furthermore, it achieves an overall 95% confidence interval for the estimated uncertainty to bound the true error. The FS method uncertainty, U_{FS}, is given by (Eq. (7)):

$$U_{FS} = FS(P)|\delta_{RE}| = \begin{cases} (2.45-0.85P)|\delta_{RE}| & 0 < P \le 1 \\ (16.4P-14.8)|\delta_{RE}| & P > 1 \end{cases} \quad (7)$$

The numerical uncertainty, U_{SN}, is composed of the iterative, U_I, grid, U_G, and time-step, U_T, uncertainties:

$$U_{SN}^2 = U_I^2 + U_G^2 + U_T^2 \quad (8)$$

Modeling errors are due to the assumptions and approximations in the mathematical representation of the physical problem, which include geometry, boundary conditions, mathematical governing equations and turbulence models. Validation procedure gives an estimation of the modeling errors, δ_{SMA}, and uncertainties, by using benchmark experimental data. The validation uncertainty, U_V, is computed as:

$$U_V^2 = U_D^2 + U_{SN}^2 \quad (9)$$

where U_D is the uncertainty of the experimental data.

The comparison error, E, is defined as the difference between the experimental data, D, and the simulation results, S:

$$E = D - S \quad (10)$$

When $|E|$ is within the $\pm U_V$ interval, the solution is validated at the U_V level, otherwise the sign and magnitude of E are used to estimate the error deriving from the modeling assumptions, δ_{SMA}.

The near-resonant physical conditions for heave motions were selected for V&V study ($Fn=0.75$, $\lambda/L_{pp}=1.806$, $Ak=0.025$), as the large ship motions, expected in this condition, make this the worst-case test. The verification parameters are the first harmonics of heave and pitch motions, A_3 and A_5, respectively, and their phases ϕ_{3_1} and ϕ_{5_1}.

4.1. Verification studies

A systematic time step converge study was carried out with a time step refinement ratio of $r_T=2^{1/2}$ on the finest grid, while a grid convergence study was conducted on the medium time step. In order to verify the mesh-independence of the solution, medium and coarse mesh were generated by coarsening the finer grid by $1/\sqrt{2}$ in each direction with a tri-linear interpolation algorithm, so that the grid distribution and shape could be as close as possible to the original shape. The resulting coarse, medium and fine grid sizes are 0.65, 1.88 and 5.4 M, respectively (Table 4).

Iterative convergence was assessed, in that the residuals of each flow variable drop four orders of magnitude after 5 iterations per time step. Furthermore, U_I values for each variable range within $0.23(\%S_1) < U_I < 0.42(\%S_1)$, so that they are negligible in comparison to the grid and time-step errors.

Results for grid and time step convergence studies are summarized in Table 5. Monotonic convergence was achieved ($0 < R_G < 1$) for A_3, A_5, ϕ_{3_1} and ϕ_{5_1}; therefore the generalized

Table 4
Grids.

	Coarse	Medium	Fine
Boundary layer1	$69 \times 31 \times 45$	$98 \times 45 \times 64$	$139 \times 65 \times 91$
Boundary layer 2	$69 \times 31 \times 45$	$98 \times 45 \times 64$	$139 \times 65 \times 91$
Background	$154 \times 69 \times 43$	$218 \times 98 \times 62$	$309 \times 139 \times 88$
Total	***649,428***	***1,889,048***	***5,424,050***

Table 5
Verification of first harmonic amplitude and phase of heave and pitch motions.

	R_G	$(p_{RE})_G$	P_G	U_G ($\%S_1$)	R_T	$(p_{RE})_T$	P_T	U_T ($\%S_1$)
A_3	0.64	1.27	0.64	5.3%	0.525	1.859	0.93	2.2%
ϕ_{3_1}	0.81	0.6	0.3	25%	0.6	1.43	0.72	6.7%
A_5	0.56	1.66	0.833	12.7%	0.44	2.36	1.18	1.67%
ϕ_{5_1}	0.83	0.53	0.27	30%	0.82	0.58	0.29	3.9%

Table 6
Validation of first harmonic amplitude and phase of heave and pitch motions.

	U_G ($\%S_1$)	U_t($\%S_1$)	U_{SN}($\%D$)	U_D($\%D$)	U_V($\%D$)	E($\%D$)
A_3	5.3%	2.2%	6.28%	2.5%	6.76%	9.38%
ϕ_{3_1}	25%	6.7%	21.2%	2.5%	21.3%	19%
A_5	12.7%	1.67%	12.76%	2.5%	13.0%	0.12%
ϕ_{5_1}	30%	3.9%	30.07%	2.5%	30.18%	3.1%

Richardson extrapolation (RE) was used in estimating the grid order of accuracy, p_G, and the grid error δ_G. The FS method was used to compute the numerical errors and uncertainties, U_G. Results show that P_G ranges within $0.3 < P_G < 0.8$, indicating that the solutions are far from the asymptotic range ($P_G=1$). Furthermore, grid uncertainties, U_G, are higher for ϕ_{3_1} and ϕ_{5_1} with respect to A_3 and A_5. The same approach was applied for the time step convergence study. The monotonic convergence between solutions was assessed ($0 < R_T < 1$). Results show that the solutions are closer to the asymptotic range for all the variables ($0.7 < P_T < 1.3$), but not pitch phase where $P_T=0.29$. The time-step uncertainties, U_T, for heave and pitch phases are higher with respect to ship motions amplitudes. By a comparison between grid and time step studies, U_G values are higher than U_T, which is relatively small. Therefore, grid errors are the significant source of numerical uncertainty.

Overall, verification results can be considered satisfactory for ship motions amplitudes, as the numerical convergence was achieved and the numerical uncertainties, U_{SN}, are consistent with previous studies involving similar flow conditions (Mousaviraad et al., 2010; Simonsen et al., 2008; Weymouth et al., 2005). On the contrary, poor accuracy in numerical predictions was achieved for phases, where high uncertainty levels were obtained, due mainly to grid resolution ($U_G=30\%$ and 25% for ϕ_{3_1} and ϕ_{5_1}, respectively). These values are much higher respect to Mousaviraad et al.(2010) ($U_G=2.77\%$ and 4.81% for ϕ_{3_1} and ϕ_{5_1}, respectively), where 22 M grid points were used in the finer grid, with respect to 5 M points used herein.

4.2. Validation studies

To determine modeling errors, the numerical results were compared to the experimental data. As the uncertainty in experimental data is not given, fairly low value of $U_D=2.5\%$ of the data was assumed. The validation uncertainty, U_V, and the comparison error, E, defined as the difference between data and the numerical value of the finer simulation ($E=D-S_1$) were calculated for A_3 and ϕ_{3_1} and for A_5 and ϕ_{5_1}. The values are summarized in Table 6.

Results show that pitch motion is validated both in amplitude and in phase. For pitch motion amplitude, A_5, in fact, the comparison error, E, is less than the validation uncertainty, U_V, hence it is validated at the U_V level of 13%D, while for pitch phase validation is achieved at an interval of 30%D. Heave phase, ϕ_{3_1}, is validated at the U_V level of 21.3%D, while heave amplitude is not validated. In this case, in fact, the comparison error, E, is 9.38%D

and is higher than the validation uncertainty value (6.76%D), i.e. modeling errors play an important role in this computation.

Results indicate that improvements are still necessary for computations involving unsteady problems. Nonetheless, the validation results can be considered encouraging for such a complicated calculation and are reasonable if compared to the literature (Mousaviraad et al., 2010; Simonsen et al., 2008; Weymouth et al., 2005), but not for phases, where U_V values are still large due to the large U_G and finer grids would be required.

5. Results

5.1. Catamaran natural frequency

The following equations are commonly used for the computation of heave and pitch natural pulsations, ω_3 and ω_5, respectively:

$$\omega_3 = \sqrt{\frac{C_{33}}{m+A_{33}}} \tag{11}$$

$$\omega_5 = \sqrt{\frac{C_{55}}{I_{55}+A_{55}}} \tag{12}$$

They are derived from the solution of the homogeneous system (no forces) of the equations of heave and pitch motions, which are explained in analogy to a mass-spring-damper system with forced motions, and are valid for monohulls in all that cases in which small and uncoupled ship motions can be assumed. C_{33} ($\rho g A_w$) and C_{55} ($\rho g I_T$) are the restoring heave force and pitch moment, A_{33} and A_{55} are the heave added mass and pitch added inertia, I_{55} is the mass moment of inertia about y axis and m is the mass of the vessel. To simplify Eqs. (11) and (12), it is assumed that $A_{55} \approx I_{55}$ and $A_{33} \approx m$. Therefore, the following formulations for natural frequency, $f_n = \omega/2\pi$, are derived for ship motions:

$$f_{n_3} = \sqrt{\frac{gC_{WP}}{8\pi^2 C_B T}} \tag{13}$$

$$f_{n_5} = \sqrt{\frac{C_{IT} g B^3}{96\pi^2 \hat{I}_{55} L_{PP}^4}} \tag{14}$$

C_{wp} is the waterplane coefficient and is calculated as $C_{WP} = (A_W/(BL_{PP}))$, where A_w is the waterplane area of the hull, B is the beam of the ship and L_{PP} is the length between perpendiculars of the ship. C_{IT} is the coefficient of inertia of the waterplane area about y axis and is computed as $C_{IT} = (12 I_T/(B^3 L_{PP}))$, where I_T is the moment of inertia of the water plane. Finally $\hat{I}_{55} = (I_{55}/\rho L_{pp}^5)$ is the non-dimensional mass moment of inertia about y axis.

The above equations, herein, were extended to twin hull, by properly defining A_w and B. A_w, in fact, is the wetted area of both hulls, B is the beam overall and C_B is the catamaran block coefficient. $f_{n3} = 1.19$ Hz and $f_{n5} = 1.28$ Hz were computed for heave and pitch natural frequencies, respectively.

In order to validate Eqs. (13) and (14) for catamarans, or multihull vessels in general, the natural frequency was also computed with calm water simulations of the catamaran free to heave and pitch with no artificial damping, and by studying the transient state before reaching the final steady sinkage and trim (Fig. 6). Three speeds were considered ($Fn = 0.45, 0.6, 0.75$) in the calculations and simulation results are shown in Table 7. Results show that the effects of the Froude number on natural frequency are negligible, in accordance with Eqs. (13) and (14), which are independent of Fn. Furthermore, heave and pitch natural frequencies, computed by the numerical simulations, coincide. In fact,

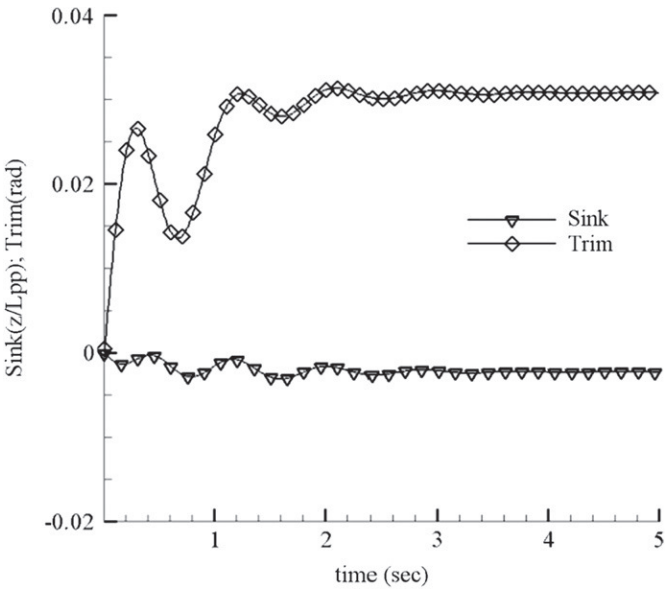

Fig. 6. Time history of ship motion amplitudes non-dimensionalized by ship length. The catamaran undergoes a transient state during which it oscillates at its natural frequency and reaches the final steady sinkage and trim values.

Table 7
Heave and pitch natural frequency as a function of ship speed.

Fn	Natural frequency (Hz)	Natural frequency (Hz)
	Heave	*Pitch*
0.45	1.32	1.32
0.6	1.30	1.30
0.75	1.28	1.28

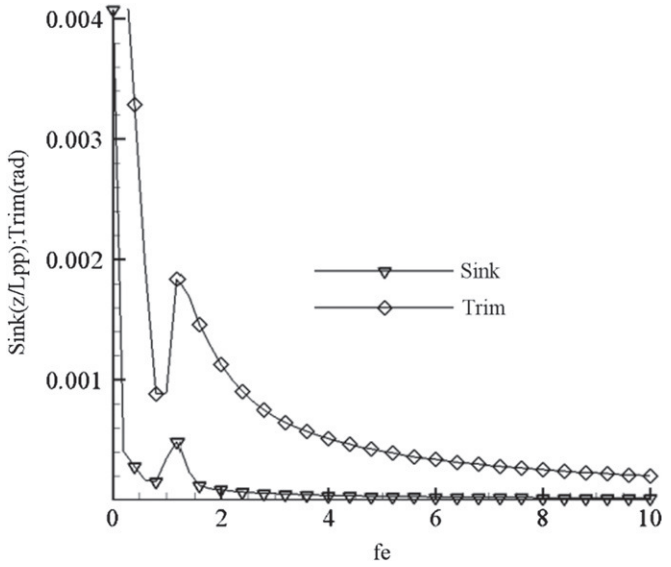

Fig. 7. Transient sink and trim responses FFT analysis as a function of encounter frequency. The peaks observed at $f_e = 1.3$ Hz are the first harmonic amplitudes of motions and occur at the catamaran natural frequency.

Fig. 6 presents the transient heave and pitch motions for $Fn = 0.6$ and the corresponding fast Fourier transform (FFT) analysis (Fig. 7) shows that the peak of the first harmonic occurs at the same frequency value for both ship motions. The average heave natural frequency, obtained by running the code, ($f_n = 1.3$ Hz),

slightly differs from the value derived from Eq. (13), which, for heave motion is approximately $f_n=1.19$ Hz, with a difference amounting to 8%. For pitch motion, better agreement is observed, as the simulations give an average natural frequency amounting to $f_n=1.3$ Hz, as for heave, against the value of $f_n=1.28$ Hz computed by Eq. (14), with an error of 1.5%. A further confirmation of the computed f_n value can be deduced from Figs. 12 and 13, where the abrupt transitions in the pitch and heave phase responses occur at $1.2 \le f_n \le 1.3$.

The above considerations allow us to conclude that, with the inclusion of the proper geometric variables, the hydrostatic estimations for heave and pitch natural frequency given in Eqs. (13) and (14), can be extended to multi-hull vessels with good accuracy.

5.2. Comparison between VERES, CFDShip and EFD

Figs. 8–11 show the numerical results of heave and pitch motions as a function of wavelength, λ/L_{pp}. RAOs are computed both by the RANS based code CFDShip-Iowa and by VERES (Stern et al., 2008), which is a strip theory based software. VERES includes both ordinary strip theory (Salvesen et al., 1970), which is valid only for the Froude numbers up to 0.4, as well as the high-speed strip theory (also referred to as "2 1/2D theory") of Faltinsen and Zhao (1991). The last one accounts for the hull interaction using the method discussed in Hermundstad et al. (1999), contrarily to conventional strip theory, where the influence of one side hull on the other hull is not accounted for. Herein, the "2 1/2D theory" was used and comparison with the available experimental data is also included. The motions are described through the transfer functions and the corresponding phases, which for heave and pitch are defined, respectively, as:

$$A_3 = \frac{x_{3_1}}{a} \tag{15}$$

$$A_5 = \frac{x_{5_1}}{ka} \tag{16}$$

where k is the wave number, a is the wave amplitude and x_{31} and x_{51} are the first harmonic of heave and pitch response whose time histories are approximated with Fourier series expansions as:

$$x_3(t) = x_{3_0} + x_{3_1}\ \cos[2\pi f t + \phi_{3_1}] + x_{3_2}\ \cos[4\pi f t + \phi_{3_2}] + x_{3_3}\ \cos[6\pi f t + \phi_{3_3}] \tag{17}$$

$$x_5(t) = x_{5_0} + x_{5_1}\ \cos[2\pi f t + \phi_{5_1}] + x_{5_2}\ \cos[4\pi f t + \phi_{5_2}] + x_{5_3}\ \cos[6\pi f t + \phi_{5_3}] \tag{18}$$

Heave and pitch motions are referred to the longitudinal center of gravity (LCG) of the ship.

In general, there is satisfactory agreement among all results. Both EFD and numerical results show the following behavior at long and short wave lengths: heave amplitude (Figs. 8a–11a) is fairly small at short wave lengths and reaches wave amplitude, A, at long wavelengths, where the transfer function A_3 approaches unity. Heave phase (Figs. 8b–11b) goes to zero at long wavelengths, i.e. there is no phase lag between heave response and wave and heave motion becomes synchronized with the incident wave. Pitch transfer function, A_5, increases towards unity at long waves (Figs. 8c–11c), where the pitch phase approaches -90° (Figs. 8d–11d), hence maximum positive pitch is registered one quarter of an encounter period after the wave trough has passed amidships. At short wave lengths, A_5 decreases towards zero and pitch phase leads increase to 180°. At the medium wavelengths

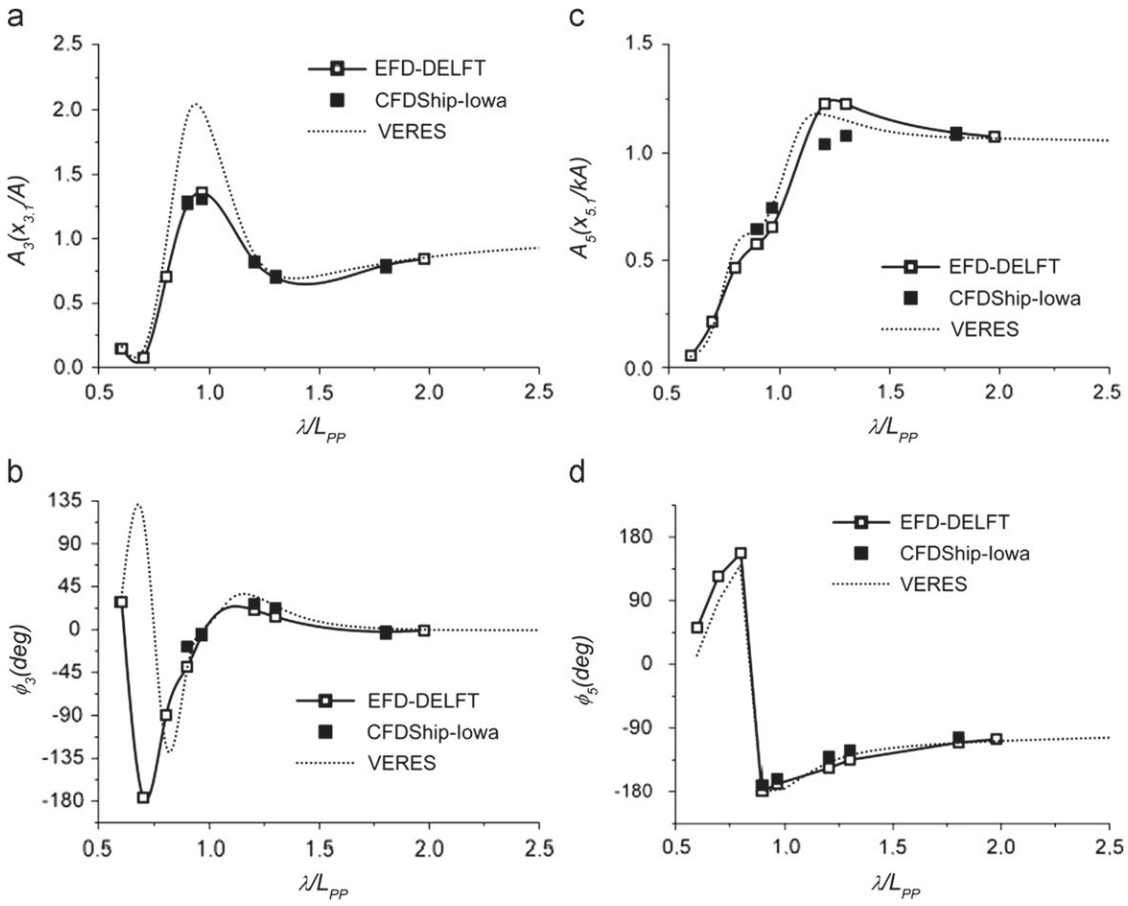

Fig. 8. Heave and pitch RAOs compared to EFD data at $Fn=0.3$: (a) heave amplitude $A_3(x_{3,1}/A)$; (b) heave phase; (c) pitch amplitude $A_5(x_{5,1}/kA)$; (d) pitch phase.

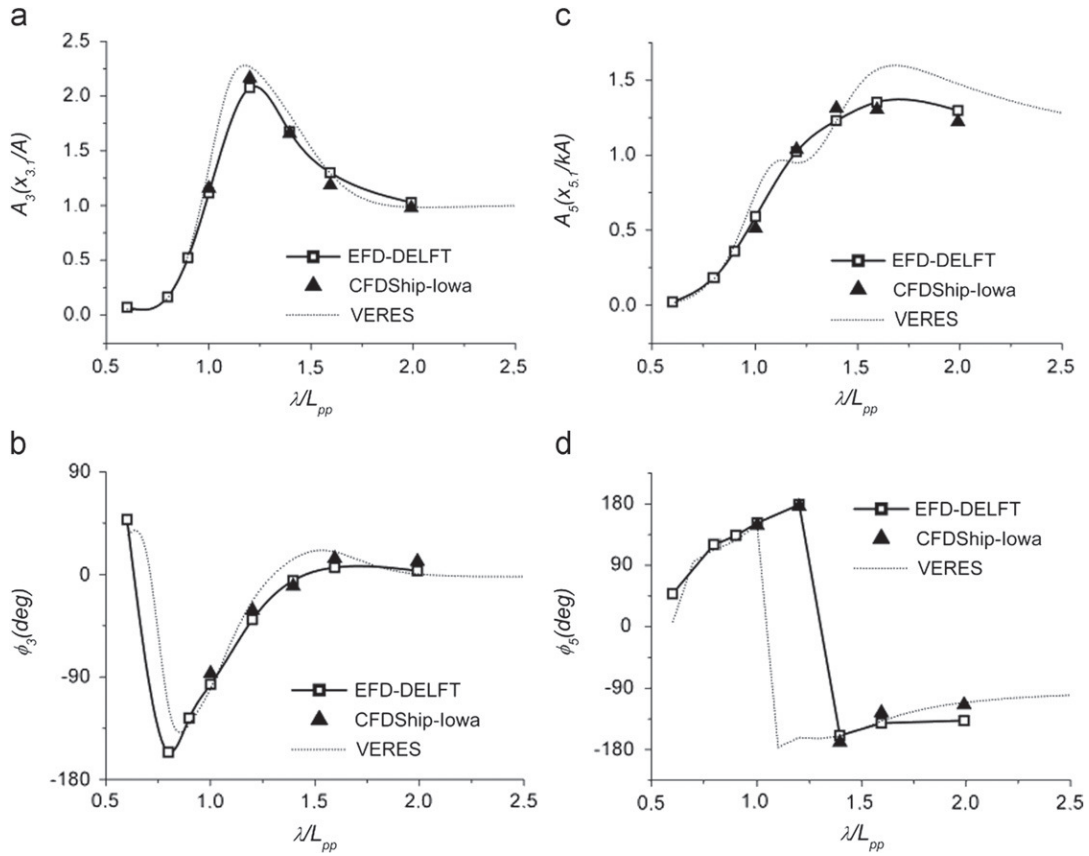

Fig. 9. Heave and pitch RAOs compared to EFD data at $Fn=0.45$: (a) heave amplitude $A_3(x_{3,1}/A)$; (b) Heave phase; (c) Pitch amplitude $A_5(x_{5,1}/kA)$; (d) Pitch phase.

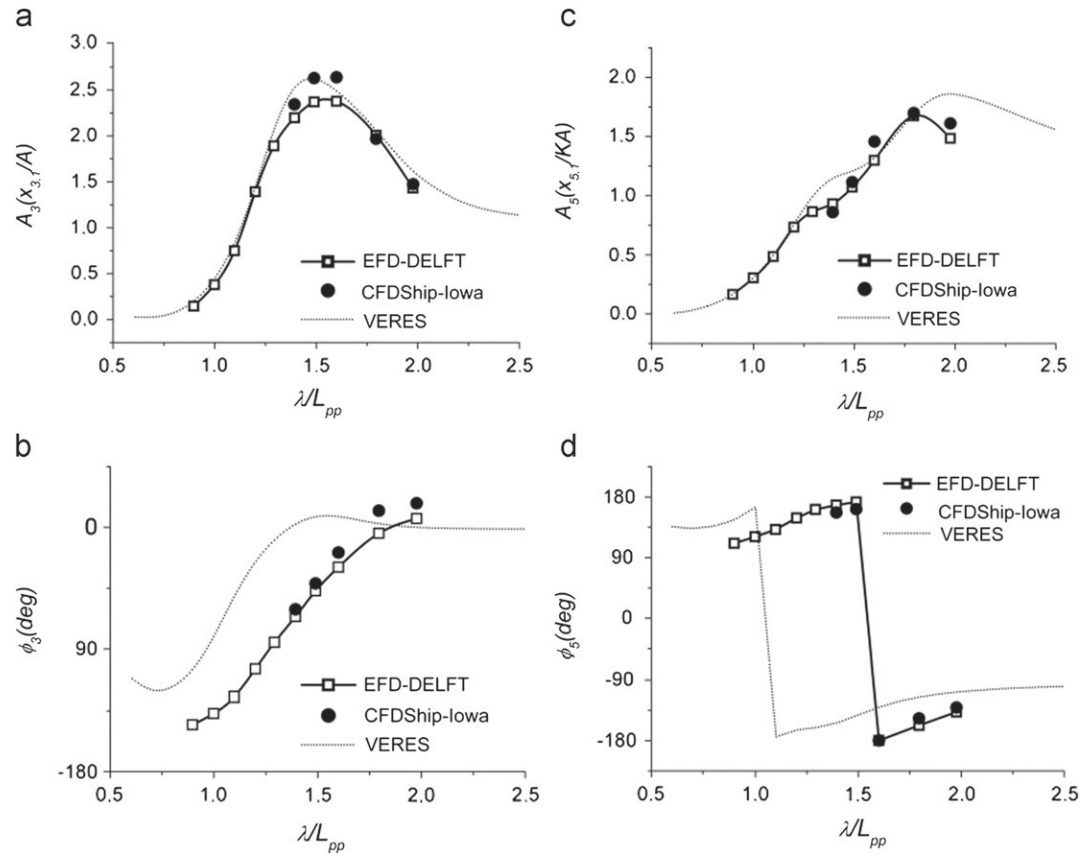

Fig. 10. Heave and pitch RAOs compared to EFD data at $Fn=0.6$: (a) heave amplitude $A_3(x_{3,1}/A)$; (b) heave phase; (c) pitch amplitude $A_5(x_{5,1}/kA)$; (d) pitch phase.

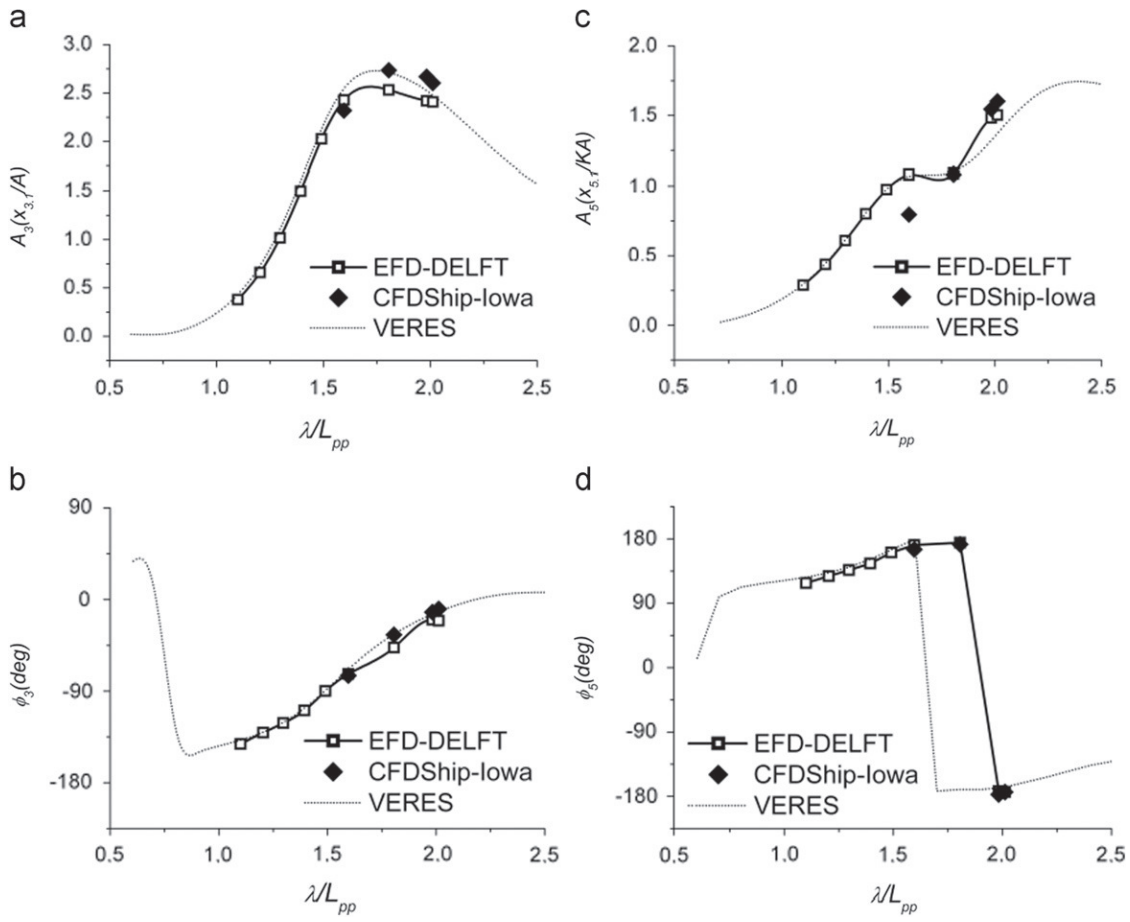

Fig. 11. Heave and pitch RAOs compared to EFD data at $Fn=0.75$: (a) heave amplitude $A_3(x_{3,1}/A)$; (b) heave phase; (c) pitch amplitude $A_5(x_{5,1}/kA)$; (d) pitch phase.

the maximum ship motions are observed, that will be discussed in more detail in the next section.

Error values are summarized in Table 8. The VERES predictions of heave and pitch amplitudes are slightly higher respect to CFDShip and to experiments, with average over-predictions, respect to EFD data, amounting to 13.92%D and to 9.63%D for heave and pitch amplitudes, respectively. The average errors of CFDShip-Iowa amount to 6.16%D for heave and to 8.27%D for pitch amplitude. The highest errors are observed near maximum ship motions, both with VERES and CFDShip. For instance, at $Fn=0.3$, where maximum A_3 occurs within $0.89<\lambda/L_{pp}<1.2$, an error of 3.82%D and 54.7%D was computed with CFDShip and VERES, respectively. Similarly, for A_5, where maximum occurs within $1.001<\lambda/L_{pp}<1.301$, errors amount to 15.24%D with CFDShip and to 29.96% with VERES. At other $Fn=0.45$, 0.6 and 0.75, errors follow similar trends as for $Fn=0.3$. With increasing Fn, VERES average errors for A_3 and A_5 decrease, while they vary slightly according to CFDShip computations. Phases show best agreement between CFDShip and EFD. VERES computations over-predict ϕ_{3_1}, with the highest differences at $Fn=0.6$, where an average error of 37.14%D was registered. More relevant discrepancies between VERES and EFD are observed for pitch phases, ϕ_{5_1}, (Figs. 8d–11d) where the abrupt transition occurs at lower wavelengths respect to EFD, for all the speed values, with average error amounting to 54.5%D, against an error of 5.9%D computed with CFDShip.

Overall, CFDShip predicts ship motions with better accuracy respect to VERES, especially in the peak zones. However, for most cases, the differences are relatively small and VERES can be considered a very useful computational tool when preliminary results and lower computational costs are required. Furthermore, comparison with previous studies involving similar conditions, as summarized in Table 9, show that errors are reasonable for most cases, and even more, for all that cases far from resonance conditions.

5.3. Maximum ship motions

Several aspects affect the maximum ship response. As discussed earlier, the wave-induced motions of a vessel are described in analogy to a mass-spring system with damping, where the excitation force is commonly given by a continuous incident wave. The dimensional encounter frequency of ship motions, f_e, is defined according to Eq. (19):

$$f_e=\sqrt{\frac{g}{2\pi\lambda}}+\frac{U}{\lambda} \tag{19}$$

When f_e, due to the incident wave length, λ, and to the ship speed, U, is close to the resonance frequency, f_n, then maximum ship motions are expected and, depending on the damping ratio, the peak is steeper or smoother. Ship motions are also affected by the exciting forces, which, according to strip theory assumptions, are estimated by the forward speed diffraction problem. Several studies, including Journee (1992), Fonseca and Soares (2004), Irvine et al.(2008), suggest that, for most cases, exciting forces give maximum response at $\lambda/L_{pp}=1.33$. This condition is considered a rough estimate and needs to be confirmed as to its dependence on geometry. Irvine et al. (2008), combined two conditions ($f_e=f_n$ and $\lambda/L_{pp}=1.33$) and estimated coincidence Fn

Table 8
Table of errors.

Fn	Ak	λ/L_{pp}	A_3 E(%D)	ϕ_{3_1} E(%D)[a]	A_5 E(%D)	ϕ_{5_1} E(%D)	Ave.
CFDSHIP							
0.3	0.0427	0.899	−1.656	−35.36	−12.111	4.572	
	0.0447	0.965	3.829	−2.99	−13.700	4.141	
	0.0323	1.204	0.923	−10.98	15.248	10.948	
	0.0288	1.301	−2.339	−15.41	12.078	10.037	
	0.0219	1.803	2.631	3.81	1.005	6.524	
|E|			***2.27***	***13.71***	***10.83***	***7.24***	***8.51***
0.45	0.038	1.001	21.09	−10.01	13.38	2.45	
	0.031	1.201	−4.19	−8.83	−1.43	1.49	
	0.027	1.396	1.06	3.15	−6.68	−5.9	
	0.022	1.595	8.8	−4.39	3.67	12.03	
	0.019	1.991	4.74	−2.44	5.77	20.96	
|E|			***7.97***	***5.76***	***6.18***	***8.56***	***7.11***
0.6	0.028	1.393	−6.63	−7.47	7.66	7.00	
	0.027	1.49	−10.91	−7.73	−4.1	6.54	
	0.025	1.6	−11.03	−4.89	−12.26	0.04	
	0.021	1.795	1.99	−22.85	−2.64	12.23	
	0.02	1.977	−2.86	−5.99	−8.55	5.03	
|E|			***6.68***	***9.78***	***7.04***	***6.16***	***7.41***
0.75	0.023	1.596	4.48	−1.71	26.15	3.69	
	0.022	1.806	−8.01	10.3	0.6	1.34	
	0.015	1.983	−10.28	8.90	5.06	−2.61	
	0.014	2.012	−8.09	13.86	4.32	−0.017	
|E|			***7.71***	***8.69***	***9.03***	***1.91***	***6.83***
			6.16	***9.48***	***8.27***	***5.96***	***7.47***
VERES							
0.3		0.601	11.1	2.70	−7.27	−75.39	
		0.699	88.15	142.72	−13.14	−27.65	
		0.803	34.94	−14.50	19.82	−10.74	
		0.899	54.69	−0.26	11.30	0.277	
		1.101	37.33	6.29	29.96	3.961	
		1.204	8.38	7.36	−4.068	−5.622	
		1.301	3.30	5.62	−6.27	−5.101	
		1.803	1.88	1.58	−2.01	0.499	
|E|			***29.97***	***22.63***	***11.73***	***16.15***	***20.12***
0.45		1.001	18.21	−3.254	29.42	−1.73	
		1.201	11.45	8.92	−9.9	−190.8	
		1.396	8.90	9.97	0.72	0.35	
		1.595	−2.42	7.08	17.45	−2.39	
		1.991	−4.37	−1.58	13.32	−19.58	
|E|			***9.13***	***5.63***	***12.79***	***36.68***	***16.06***
0.6		1.098	8.8	54.54	1.59	−232.3	
		1.2	1.94	58.105	2.88	−210.1	
		1.292	14.36	56.3	19.68	−199.3	
		1.393	18.79	50.50	25.28	−191.19	
		1.49	11.56	40.506	12.52	−182.16	
		1.6	5.22	27.36	0.34	−27.41	
		1.795	2.17	4.99	3.32	−26.94	
		1.997	8.49	−4.82	26.49	−22.15	
|E|			***8.91***	***37.14***	***11.51***	***136.44***	***48.5***
0.75		1.1	10.68	−2.9	1.29	6.83	
		1.204	5.71	0.31	−1.35	3.38	
		1.297	8.75	−0.43	1.4	3.09	
		1.394	8.92	−2.14	2.92	4.38	
		1.491	8.74	−1.91	3.23	3.22	
		1.596	7.03	−4.71	0.51	4.63	
		1.806	7.68	−10.54	−0.36	−197.53	
		1.983	3.89	−6.19	−8.87	−2.77	
			7.67	***3.64***	***2.49***	***28.8***	***10.65***
			13.92	***17.26***	***9.63***	***54.51***	***23.83***

[a] % dynamic range.

when global maximum response may occur, as:

$$Fn_{coincidence} = 1.33\left[\sqrt{\frac{L_{pp}}{g}}f_n - \sqrt{\frac{3}{8\pi}}\right] \quad (20)$$

Eq. (20) was derived both for heave and pitch, and is valid only for head waves. Furthermore, the effects of high Froude numbers and multi-hull vessels are not included. In order to verify Eq. (20) and to investigate maximum response conditions, Simonsen et al. (2008) designed a test program for the KCS, including speed values higher than the coincidence *Fn*. They tested the KCS containership at $Fn=0.26$, 0.33 and 0.40 for wavelength range of $\lambda/L=0.5$–2.0 with constant wave steepness of $Ak=0.0525$. In accordance with Irvine et al.(2008), they found that both heave and pitch the transfer functions increase with speed, being maximum at the highest speed, i.e. $Fn=0.4$. For heave, the maximum response for all three speeds occurs at resonance, while for pitch it occurs at different frequencies, all smaller than resonance. At fixed $\lambda/L_{PP}=1.33$, local maximum heave response occurs for $fe\sim fn$, i.e. at the coincidence $Fn=0.33$, but the maximum pitch response occurs at lowest $Fn=0.26$. Finally, the maximum response occurs at the coincidence *Fn* for added resistance.

Table 9
Summary of previous URANS CFD studies.

	Geometry	Fn	Ak	λ/L_{pp}	Variable	|E(%D)|
Mousaviraad et al. (2010)	DTMB 5512	0.19–0.41	Gaussian amplitude distribution	Various	A_3	4.9
					ϕ_{3_1}	1.39
					A_5	2.91
					ϕ_{5_1}	4.66
Stern et al. (2008)	DELFT-Cat	0.6	0.025-0.05	1.6-1.9	A_3	5.63
					A_5	5.99
Simonsen et al. (2008)	KCS	0.26	0.0525	1.15	A_3	4.7
					A_5	11
Carrica et al. (2007a,b)	DTMB 5512	0.41	0.025	1.5	A_3	2.8
					ϕ_{3_1}	2.8
					A_5	5.1
					ϕ_{5_1}	3.2

In order to focus on the maximum response conditions for the catamaran, a summary of the catamaran RAOs as a function of the encounter frequency (f_e) and of the wave length (λ/L_{pp}), for all *Fn*, is presented in Figs. 12 and 13, for heave and pitch motions, respectively. According to Eq. (20), the coincidence *Fn* for the catamaran is $Fn_{coincidence}=0.49$. Similar to KCS, heave peaks occur at resonance ($f_e=f_n=1.3$ Hz) for all *Fn* (Fig. 12a), and increase with speed, reaching the absolute maximum at the highest speed ($Fn=0.75$). However, if A_3 is plotted as a function of wavelength (Fig. 12c), heave peaks occur at different λ/L_{PP} values, depending on *Fn*. Also, similar to KCS, maximum pitch (Fig. 13a) occurs at different frequencies, all lower than resonance, for each speed, but the absolute maximum seems to occur at medium *Fn*, i.e. $Fn=0.6$. However, both experimental data and numerical results lack information at the lowest frequencies for $Fn=0.75$ and further investigation is required in order to detect the peak value. In Fig. 13c), where pitch amplitude is plotted versus wavelength, the peaks are reached at different λ/L_{PP} value, varying with *Fn*. Furthermore, also for the catamaran, as will be discussed in Section 5.5.2, the maximum added resistance occurs at $Fn=0.45$, which is, interestingly, near the coincidence $Fn_{coincidence}=0.49$.

Overall, our results seem to be consistent with estimation of maximum response conditions as found in Simonsen et al. (2008), though herein, a different geometry and much higher *Fn* were tested. Nonetheless, some disagreement with Eq. (20) is observed, in that global maxima occur at higher *Fn* respect to coincidence condition, that needs, therefore, further investigation in order to clarify the effects of geometry and of maximum exciting forces on heave and pitch in head waves.

5.4. Effects of wave steepness on ship response

The assumption of linear response of ship motions with wave amplitude is usually made in seakeeping studies. This approach is

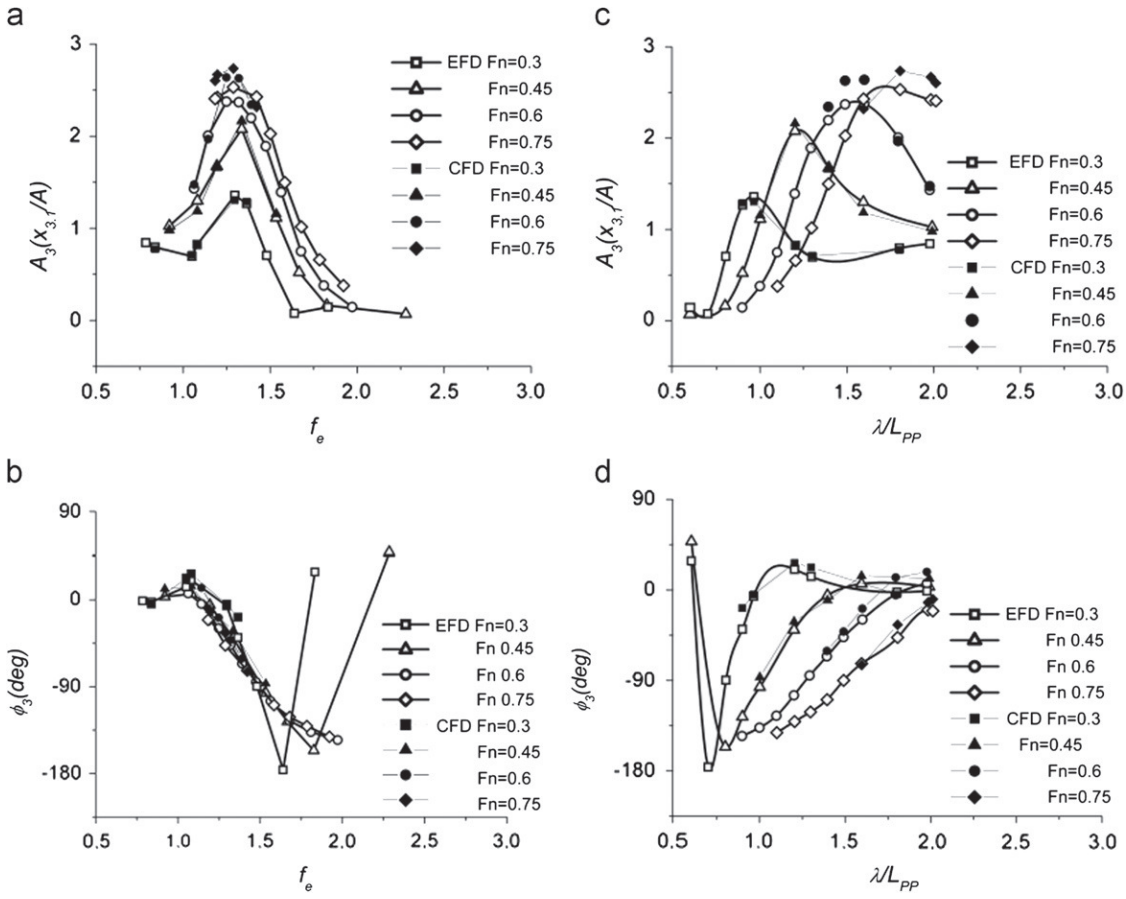

Fig. 12. Heave RAOs at $Fn=0.3$, 0.45, 0.6 and 0.75: (a) amplitude $A_3(x_{3,1}/A)$ as a function of the encounter frequency, f_e; (b) phase (deg) as a function of f_e; (c) amplitude $A_3(x_{3,1}/A)$ as a function of the wave length, λ/L_{pp}); (d) phase (deg) as a function of λ/L_{pp}.

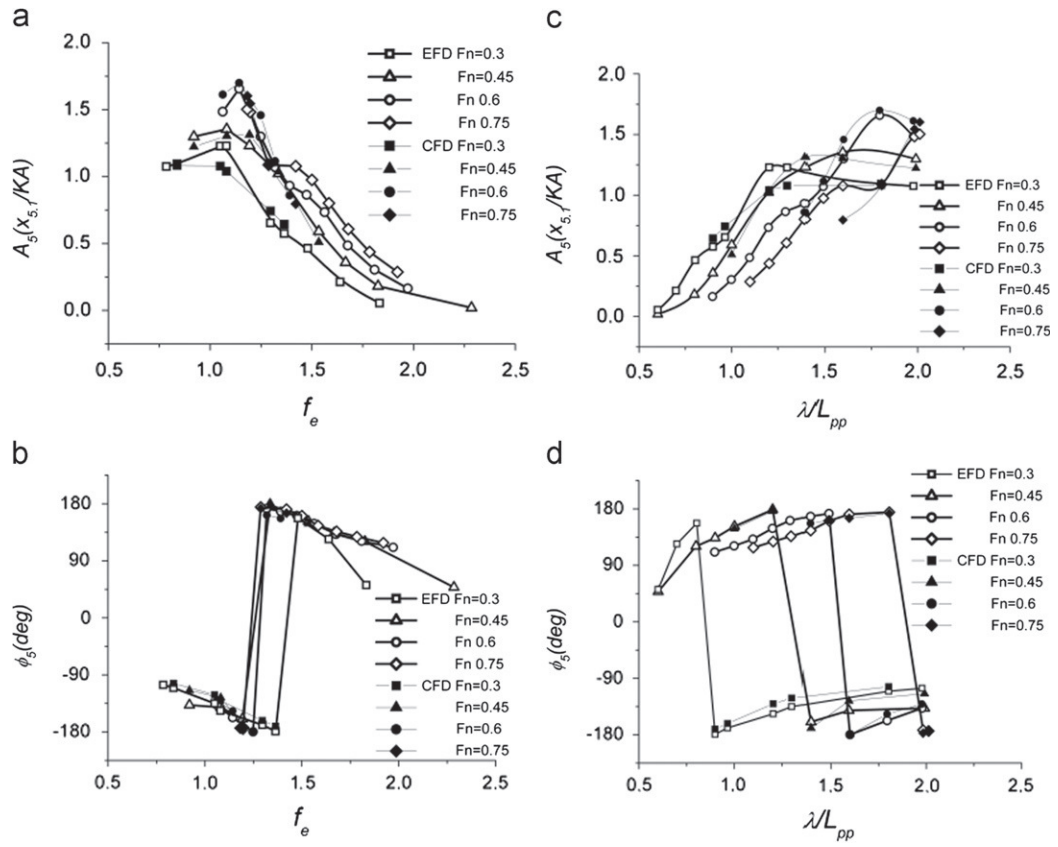

Fig. 13. Pitch RAOs at $Fn=0.3$, 0.45, 0.6 and 0.75: (a) amplitude $A_5(x_{5,1}/kA)$ as a function of the encounter frequency, f_e; (b) phase (degrees) as a function of f_e; (c) amplitude $A_5(x_{5,1}/kA)$ as a function of the wave length, λ/L_{pp}); (d) phase (deg) as a function of λ/L_{pp}.

very useful because the more realistic motions in irregular waves can be represented by the superposition of the different facets of the wave–body interaction in regular waves. However, this assumption requires sufficiently small wave amplitudes to justify linearization.

In order to evaluate the range of steepness values in which a linear behavior of the catamaran can be assumed, simulations were performed for different steep waves with CFDShip-Iowa. Specifically, the simulations were carried out for $Fn=0.75$, where maximum response occurs, at the steepness values of 0.025, 0.05 and 0.1 (Table 3). Differently, VERES is a linear code, therefore computations are independent of wave amplitude.

Results are shown in Fig. 14, where the first harmonic amplitudes and phases of heave and pitch motions are plotted as a function of the wavelength for several Ak values. At low steepness, i.e. $Ak=0.025\div0.05$, there is good agreement between VERES, CFDShip and experimental data. For heave motion (Fig. 14a), the numerical results are Ak-independent in the whole range of the tested wavelengths and heave motion shows, therefore, a linear behavior. As Ak increases, CFDShip results show a sensitivity to wave amplitude, with a reduction of heave amplitude amounting to 28% near the peak, and higher differences with VERES occur. Ship response, in this case, is nonlinear. Similar behavior is observed for heave phases (Fig. 14b). For pitch motion amplitudes (Fig. 14c), nonlinearity seems to occur over the whole range of wavelengths and amplitudes under observation. However, pitch angles are quite small (2°–3°) and differences are not high enough to be appreciable. Furthermore, the peak pitch response reduces of 46%, with increasing steepness.

Experimental data for high steep waves are not available for the DELFT catamaran. However, numerical results are consistent with EFD data available in the literature for different geometries. In fact, O'Dea et al. (1992), who focused on a 3.5 m containership model ITTC S-175, observed nonlinearities in ship response for $Ak>0.08$ and approximately linear response for $Ak<0.08$. Furthermore, a reduction in the peak heave and pitch responses by up to 25–50%, with increasing wave steepness, were observed. Also Fonseca and Soares (2004) investigated nonlinear vertical plane motions for a 4.4 m model ITTC S-175. Their results show nonlinear heave and pitch motions for $Ak>0.07$ and approximate linear response for $Ak<0.07$. Results, also in this case, show a reduction of peak heave and pitch response of up to 20–25% with increasing wave steepness. Carrica et al. (2007a,b) found a reduction in transfer functions amounting to 41% for heave and to 27% for pitch. Finally, the results of Irvine et al. (2008), for the DTMB model 5512, show that the transfer functions and phases of the vertical plane motions are linear or Ak-independent, in the range of tested Ak values ($0.025<Ak<0.075$).

5.5. Catamaran resistance in waves

Evaluation of added resistance in waves is an important issue in seakeeping studies, as it can represent a relevant component over the total resistance (~30%, depending on the waves height). Added resistance is a consequence of the interaction between incident waves and the ship and it is caused by their relative motion. The highest relative motions between the hull and the waves are usually registered near resonance, as was observed also in the section of ship motions. Under these conditions, a peak of added resistance is usually expected. For lower wavelengths, ($\lambda/L_{pp}<0.5$), where the ship motions are limited, the waves are reflected by the hull and a finite component of added resistance is expected. Finally, when wavelengths are very large, the relative motion between the hull and the waves is negligible and the added resistance component goes to zero. Added resistance

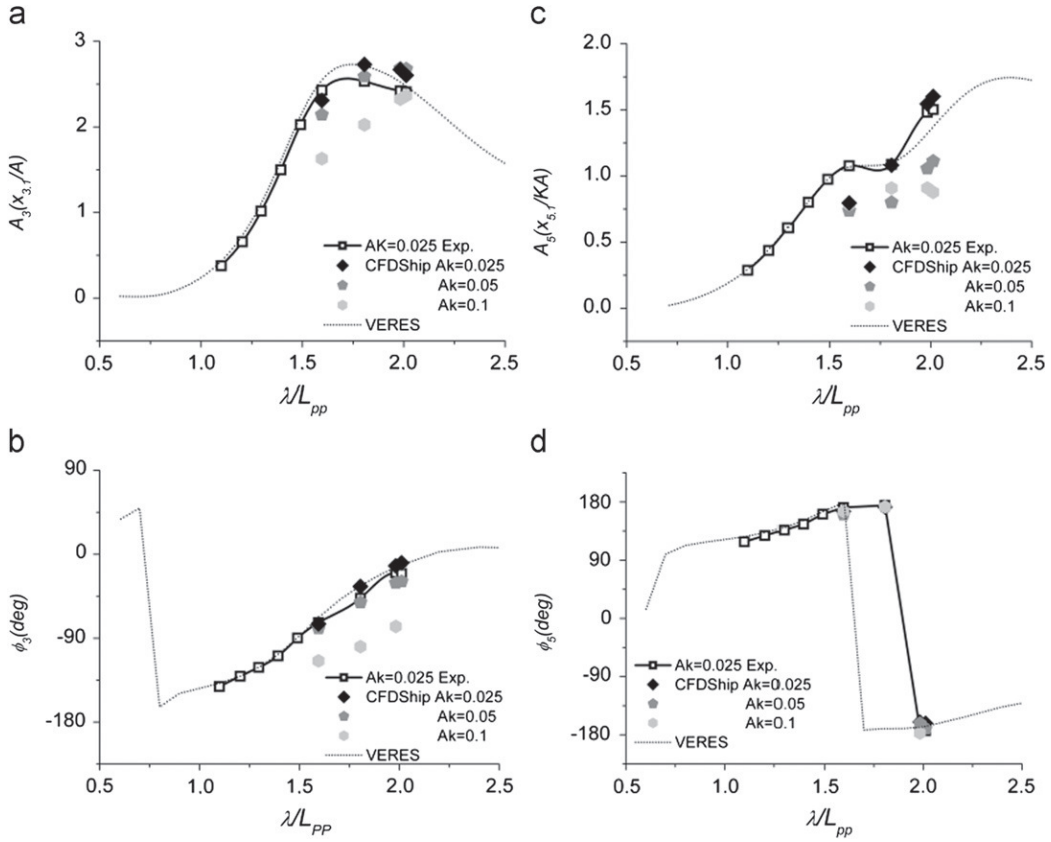

Fig. 14. Computational results for estimating the effects of wave steepness on ship response for $Fn=0.75$. $Ak=0.025,0.05,0.1$: (a) heave RAOs; (b) heave phases; (c) pitch RAOs; (d) pitch phases.

evaluation is based on the following equation:

$$R_{aw} = R_{T0} - R_{Tcalmwater} \quad (21)$$

where $R_{Tcalmwater}$ is resistance in calm water and R_{T0} is mean value of resistance in waves. Furthermore, R_{aw} is normalized by $\rho g A^2 (B^2/L)$ as added resistance is a streaming value, i.e. second order term, and it can be non-dimensionalized by A^2.

In order to calculate the added resistance for the DELFT catamaran and its dependence on wavelength and wave amplitude, evaluation of resistance is needed both in waves and in calm water and the results will be discussed in the following sections.

5.5.1. Calm water tests

Experimental results are available for resistance, sinkage and trim for the catamaran advancing in calm water, in a speed range going from $Fn=0.18$–0.75. The following conventions are used for ship motion: trim is positive bow up, while sinkage is negative when the ship moves down the free surface at rest.

Numerical computations were performed at the same EFD conditions and the results are compared in Fig. 15. The resistance curve is quite well predicted, while, for sinkage and trim, higher differences occur between numerical results and experiments. The comparison error, $|E|$, for total resistance coefficient is included in the range 0.8–9.5%D, while for sinkage it is about 11–26% and for trim it is about 6–26%.

Fig. 16 illustrates the surface pressure and wave elevation for three Froude numbers (0.3, 0.55, 0.7) and it is helpful to have a better understanding of the relationship between resistance, sinkage and trim curves. Owing to the symmetry of the problem, only results for one hull are illustrated and the interference effects between the wave systems generated by both hulls, are observed in the inner region, with more pronounced crests and troughs with respect to starboard. $Fn=0.55$ is the speed value corresponding to the C_t peak. At this speed, in fact, high suction pressures, owing to wave trough interference at the stern, can be observed. At $Fn=0.3$, the suction pressures decrease, while, at $Fn=0.7$ the wave trough goes beyond the stern, with limited effects on the hull surface. Trim angle, which is caused by the difference in pressure distribution between the bow and the stern, follows a similar trend as C_t. In fact, at $Fn=0.55$, the pressure difference between bow and stern is more relevant than in the other two cases. The pressure distribution also affects sinkage. In fact, sinkage values are negative in the whole range of speeds under study. This is due to the net negative hydrodynamic forces acting on the hull wetted surface and are generated by the wave troughs and by their suction effects on the center of gravity below the free surface. The sinkage maximum can be observed at $Fn=0.55$, where the highest suction pressure acts on the whole stern area. In the other two cases, both area and pressure values are more limited.

5.5.2. Added resistance in waves

Preliminary evaluation of added resistance, as a function of the Froude number, is given in Fig. 17, where comparison between C_t computed in calm water and in waves is presented. Total resistance coefficient in waves, for each Froude number, was derived as averaged values over time and wavelength. Results show that the added resistance in waves is significant for low ship

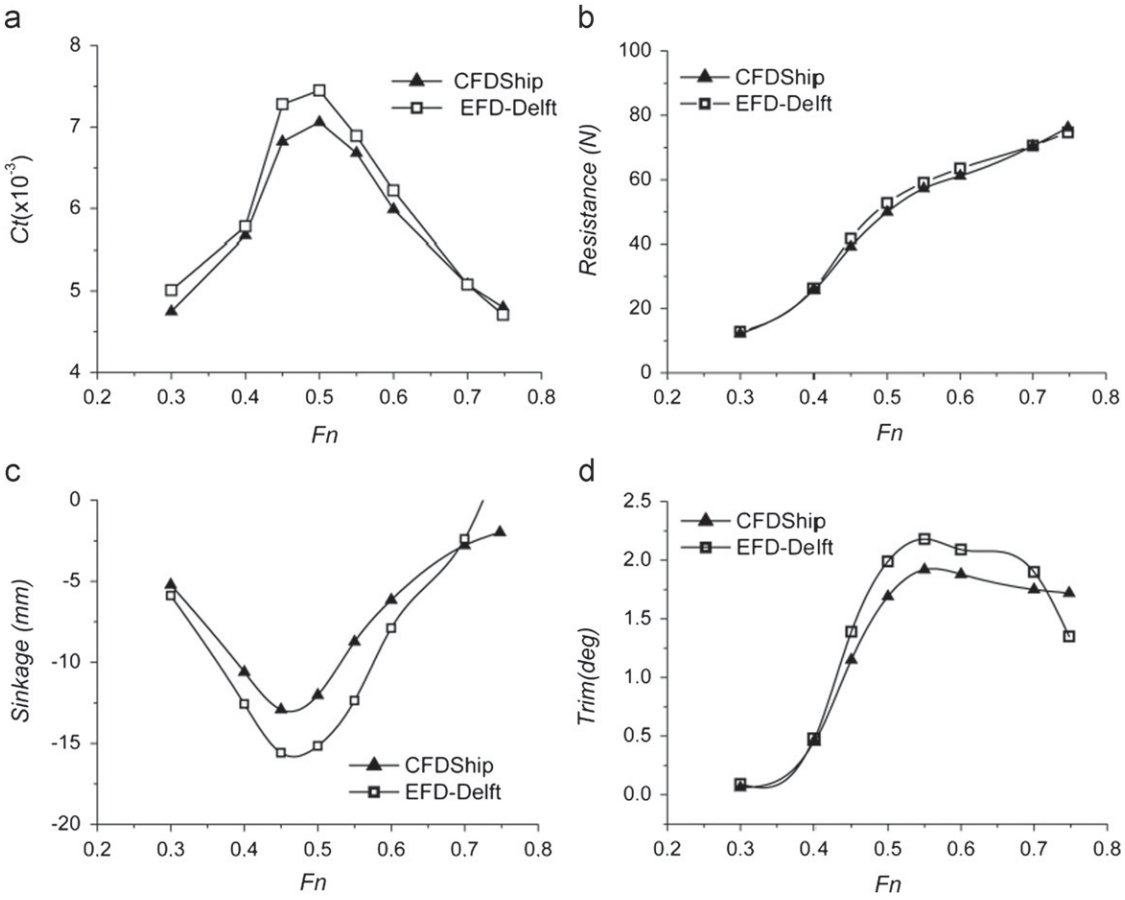

Fig. 15. Catamaran advancing in calm water. Comparison between experimental data and calculated values as functions of the Froude number, *Fn*: (a) total resistance coefficient; (b) resistance (N); (c) sinkage (mm); (d) trim angle (deg).

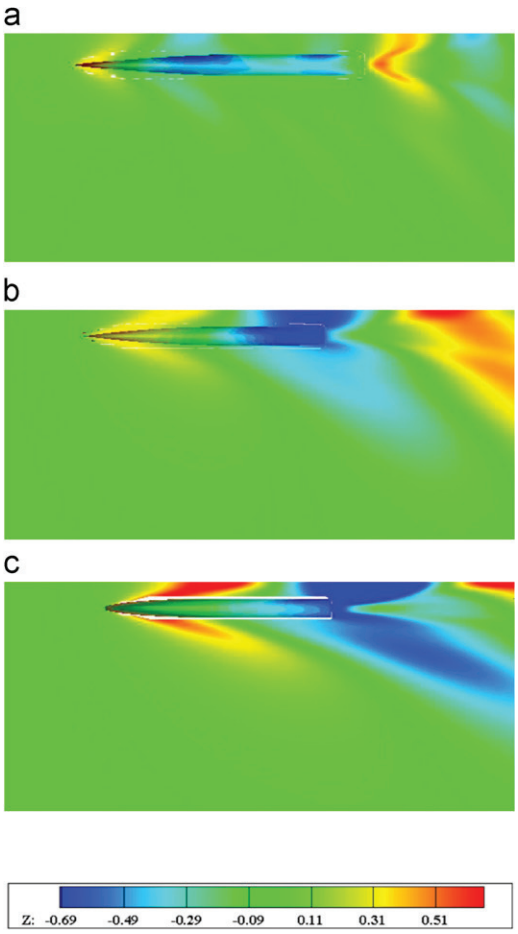

Fig. 16. Wave elevation and pressure distribution on the hull surface for the catamaran advancing in calm water: (a) $Fn=0.3$; (b) $Fn=0.55$; (c) $Fn=0.7$.

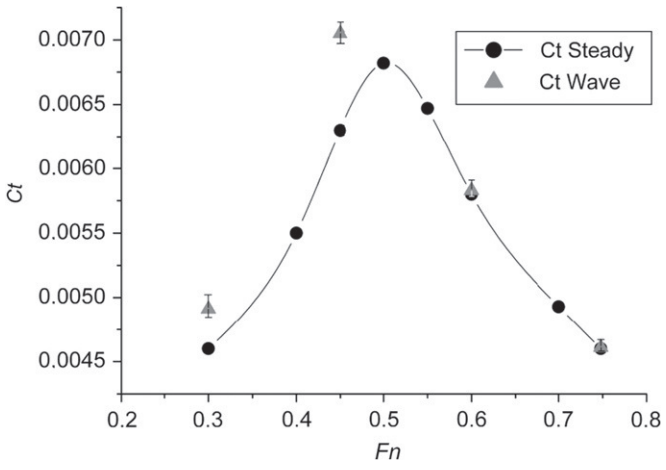

Fig. 17. Comparison between calculated C_t values in calm water and in waves as function of Fn; C_T in waves, for each Fn, is derived as averaged values over wavelength. At each Fn, bars show the range of C_T values about mean value. δC_t is significant at low speed values ($Fn \leq 0.5$) while it is negligible at high Fn values.

speeds ($Fn \leq 0.5$), while it is negligible for higher Fn values. Maximum R_{aw} was computed at $Fn=0.45$ where an increase of 10% was registered over its calm water value. It seems interesting to observe that $Fn=0.45$, where maximum added resistance occurs, is close to the coincidence Fn, which for the catamaran, according to Eq.(20), is $Fn_{coincidence}=0.49$. This result is in good agreement with Simonsen et al. (2008), who found maximum added resistance at $Fn_{coincidence}$ for the KCS, though lower Fn than catamaran were tested.

At each Fn, added resistance was also computed according to Eq. (21) for all frequencies and results are plotted in Fig. 18. For each Fn, added resistance is maximum at $f_e \approx 1.3$, i.e. at resonance, where the highest relative motions between the hull and the waves are registered. Furthermore, this component goes to zero at low frequency values, where the relative motion between the hull and the waves is negligible. This behavior is consistent with literature (Stern et al., 2008; Faltinsen and Zhao, 1991) and confirms the strong relation between added resistance and ship motions.

As previously mentioned, added resistance is a streaming value as it is defined as the difference between the steady and 0th-order harmonic component of resistance. Therefore, it is a second order/nonlinear term. Added resistance has been expressed in terms of the added resistance operator, defined as $\delta C_t/A^2$, where δC_t is the increase in drag coefficient over its calm-water value and A is the wave amplitude. It was calculated for the highest speed value ($Fn=0.75$) at three different wavelengths ($\lambda/L_{pp}=1.596$, 1.806 and 2.012) and three steepness values ($Ak=0.025$, 0.05 and 0.1). Results are plotted in Fig. 19. It illustrates that for the highest wavelength value ($\lambda/L_{pp}=2.012$), the added resistance is weakly more than quadratic

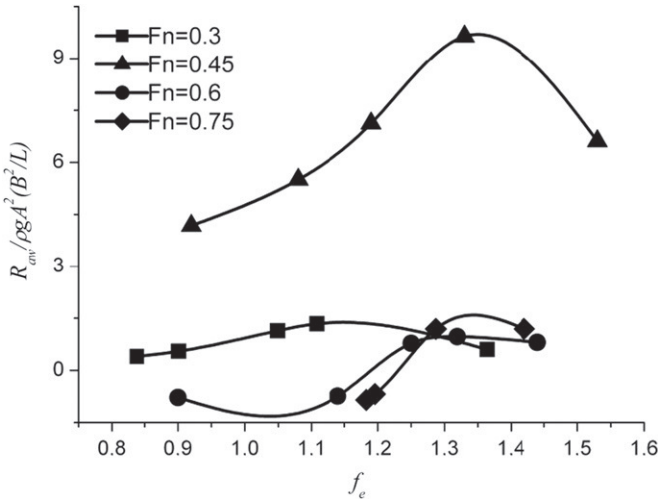

Fig. 18. Non-dimensional added resistance as a function of the encounter frequency f_e.

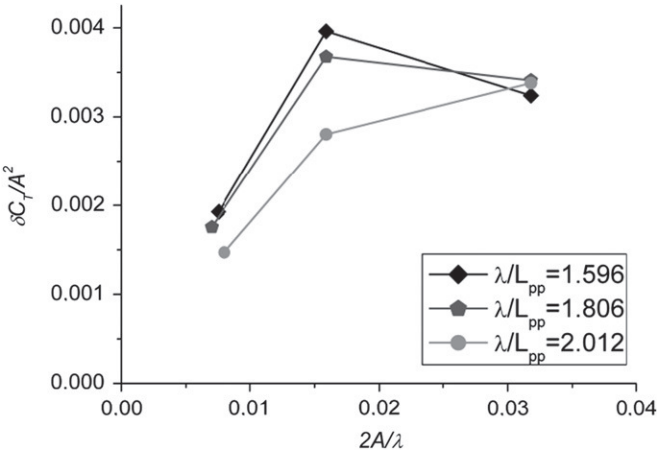

Fig. 19. Calculated C_t operator ($\delta C_t/A^2$) as function of steepness ($2A/\lambda$) for different wavelengths.

with wave amplitude. As the wavelength decreases, the gap from quadratic dependence of δC_T on A is more severe and this reflects the response of ship motions that is nonlinear with wave steepness at the lower wavelengths. Quite similar results were observed in computations on a trimaran, made by Stern et al. (2003), who computed the added resistance operator for three wavelengths (λ/L_{pp}=1.2.1.4 and 1.6) and three steepnesses ($2A/\lambda$=1/120, 1/60 and 1/30). Results show that the added resistance is close to quadratic with wave amplitude for longer waves, while, at the shorter wavelengths the operator is not independent of steepness, although variation with steepness only becomes severe for very steep waves. Their results also show that the operator increases as wavelength decreases, in accordance with the results shown in Fig. 19.

6. Conclusions

In this work, the seakeeping behavior of a catamaran advancing in regular waves was investigated numerically by the Unsteady RANS code CFDShip-Iowa V.4.

The present results demonstrate that CFD, based on Unsteady RANS, is a valid tool in the simulation of seakeeping problems involving complex flow conditions (high ship speeds, high sea states). Ship motions, in fact, were predicted with reasonable accuracy for most cases, while higher comparison errors between experimental and calculated values were registered at resonant conditions. Verification study at resonance proved that the grid quality was the major source of numerical errors, while validation was achieved for all variables but for heave amplitude.

With regard to the response of the catamaran to the incoming regular head waves, the study of several aspects was undertaken. Validation of an equation for the computation of catamaran natural frequency was achieved. Maximum heave motion occurred at resonance ($f_e=f_n$) for the whole range of the tested Froude numbers and it increased with speed, reaching its global maximum at the highest speed (Fn=0.75). Maximum pitch motion was observed for an encounter frequency lower than resonance and it increased with speed, reaching its maximum at Fn=0.6. This behavior is in good agreement with literature, though herein, multi-hull geometry and higher Fn values were tested. Differently to literature, it was observed that there is not any correlation between maximum response condition and exciting loads at λ/L_{PP}=1.33. However, this aspect requires further investigation and CFD results could be helpful in the evaluation of exciting forces and their correlation with f_e and λ/L_{PP}.

A linear response of the catamaran was obtained for low steep waves ($Ak \leq 0.05$), in the range of wavelengths under consideration (λ/L_{PP}=1.6–2.012), where good correlation between viscous computations, strip theory results and EFD data was achieved. Nonlinear effects were detected by viscous computations at the highest steep waves (Ak=0.1), where reduction of ship response occurred and the differences with strip theory results were relevant. Concerning the added resistance in waves, results show maximum R_{aw} at Fn=0.45 and it reduces with increasing ship speed. Interestingly, this value is close to $Fn_{coincidence}$=0.49 computed for the catamaran. Furthermore, maximum added resistance occurs at resonance for all Fn. Finally, the added resistance shows a quadratic dependence on wave amplitude for all the cases where linear ship motions were registered.

A relevant aspect to consider in future research could be the study of nonlinearities of ship motions both from a computational and an experimental point of view. In the literature, in fact, the number of studies, dealing with this aspect, is quite limited and the analysis made herein was limited owing to a lack of experimental data.

Acknowledgments

Partially supported ONR Grant N00014-01-1-0073 under the administration of Dr. Patrick Purtell. Special thanks are extended to Mike Hughes for help with additional results and comments on VERES.

References

Carrica, P., Wilson, R.V., Stern, F., 2006. Unsteady RANS simulation of the ship forward diffraction problem. Computers & Fluids 35, 545–570.

Carrica, P., Wilson, R.V., Stern, F., 2007a. An unsteady single-phase level-set method for viscous free surface flows. International Journal of Numerical Methods in Fluids 53 (2), 229–256.

Carrica, P., Wilson, R.V., Noack, R.W., Stern, F., 2007b. 'Ship motions using single-phase level set with dynamic overset grids'. Computers & Fluids 36, 1415–1433.

Cura Hochbaum, A. & Vogt, M. (2002). Towards the simulation of seakeeping and maneuvering based on the computation of free surface viscous ship flow. In: Proceedings of the 24th Symposium on Naval Hydrodynamics, Fukoka, Japan.

Faltinsen, O.M., Zhao, R., 1991. Numerical predictions of ship motions at high forward speed. Philosophical Transactions of Royal Society of London A 334, 241–257.

Fonseca, N., Soares, C.G., 2004. Experimental investigation of the non-linear effects on the statistics of vertical motions and loads of a containership in irregular waves. Journal of Ship Research 48, 118–147, 148–167.

Hermundstad, O.A., Aarsnes, J.V., Moan, T., 1999. Linear, hydroelastic analysis of high-speed catamaran and monohulls. Journal of Ship Research 43 (1), 48–63 March 1999.

Irvine, M., Longo, J., Stern, F., 2008. Pitch and heave tests and uncertainty assessment for a surface combatant in regular waves. Journal of Ship Research 52, 146–163.

Journee, J.M.J. (1992) Experiments and calculations on four Wigley Hullforms, Delft University of Technology, Ships Hydrodynamic Lab, Report N 909.

Korvin-Kroukovsky, B.V., Jacobs, W.R., 1957. Pitching and heaving motions of a ship in regular waves. Transactions of SNAME 65, 386–435.

Larsson, L., Stern, F. & Bertram, V. (2000). 'Gothenburg 2000: a workshop on numerical Ship Hydrodynamics', Gothenburg, Sweden.

Mousaviraad, M.S., Carrica, P., Stern, F., 2010. Development and validation of harmonic wave group single-run procedure for RAO with comparison to regular wave and transient wave group procedures using URANS. Ocean Engineering 37, 653–666.

Noack, R. (2005). SUGGAR: a general capability for moving body overset grid assembly. AIAA paper 2005-5117, 17th AIAA Computational Fluid Dynamics Conference, Ontario, Canada.

O'Dea, J.,Powers, E., Zselecsky, J. (1992). Experimental determination of non-linearities in vertical plane ship motions. In: Proceedings of the 8th International Conference on Numerical Ship Hydrodynamics, Busan, Korea.

Ogilvie, T.F. & Tuck, E.O. (1969) A Rational Strip-Theory of Ship Motion: Part I, Department of Naval Architecture, The University of Michigan, Report No.013.

Orihara, H., Miyata, H. (2003). A numerical method for arbitrary ship motions in arbitrary wave conditions using overlapping grid system. In: Proceedings of the 19th ONR Symposium on Naval Hydrodynamics, Seoul, Korea.

Salvesen, N., Tuck, E.O., Faltinsen, O., 1970. Ship motions and sea loads. Transactions of the Society of Naval Architects and Marine Engineers 78, 250–287.

Sato, Y., Miyata, H., Sato, T., 1999. CFD simulation of 3-dimensional motion of a ship in waves: application to an advancing ship in regular head waves. Marine Science and Technology 4, 108–116.

Simonsen, C., Otzen, J. & Stern, F. (2008). ' EFD and CFD for KCS heaving and pitching in regular head waves'. In: Proceedings of the 27th Symposium on Naval Hydrodynamics, Seoul, Korea.

Stern, F., Wilson, R., Longo, J., Carrica, P., Xing,T., Tahara, Y., Simonsen, C., Kim, J., Shao, J., Irvine, M., Kandasamy, M., Ghosh, S., Weymouth, G. (2003). Paradigm for development of simulation based design for ship hydrodynamics. The 8th International Conference on Numerical Ship Hydrodynamics, Busan, Korea.

Stern, F., Wilson, R., Shao, J., 2006. Quantitative approach to V&V of CFD simulations and certification of CFD codes. International Journal for Numerical Methods in Fluids 50, 1335–1355.

Stern, F., Carrica, P., Kandasamy, M., Ooi, S.K., Gorski, J., O'Dea, J., Fu, T., Hendrix, D., Kennell, C., Hughes, M., Miller, R., Marino, T., Hess, D., Kring, D., Milewski, W., Hoffman, R., Smith, S., Cary, C., Taylor, P., Paterson,B., Harris, D., and Monaco, C.. Computational hydrodynamic tools for high-speed sealift: phase ii final report. IIHR Report No. 465, Iowa Institute of Hydraulic Research, The University of Iowa, Iowa City, 2008.

Timman, R., Newman, J.N., 1962. The coupled damping coefficients of symmetric ships. Journal of Ship Research 5 (2), 1–7.

Van't Veer, R. (1998a). Experimental results of motions, hydrodynamic coefficients and wave loads on the 372 Catamaran model. Delft University Report 1129.

Van't Veer, R. (1998b). Experimental results of motions and structural loads on the 372 Catamaran model in head and oblique waves. Delft University Report 1130. VERES User Manual, Marintek, 2003.

Weymouth, G.D., Wilson, R.V., Stern, F., 2005. RANS computational fluid dynamics predictions of pitch and heave ship motions in head seas. Journal of Ship Research 49, 80–97.

Wilson, R.V., Carrica, P., Stern, F., 2005. Unsteady RANS method for ship motions with application to roll for a surface combatant. Computers & Fluids 35, 501–524.

Xing, T., Carrica, P., Stern, F., 2008. Computational towing tank procedures for single run curves of resistance and propulsion. ASME Journal of Fluids Engineering 130, 101102.

Xing, T., Stern, F., 2010. Factors of safety for Richardson extrapolation. Journal of Fluids Engineering, 132.